Libration Point Orbits and Applications
G. Gómez, M. W. Lo and J. J. Masdemont (eds.)

LIBRATION POINT ORBITS: A SURVEY FROM THE DYNAMICAL POINT OF VIEW

G. GÓMEZ

IEEC & Departament de Matemàtica Aplicada i Anàlisi
Universitat de Barcelona, Gran Via 585, 08007 Barcelona, Spain

J.J. MASDEMONT and J.M. MONDELO

IEEC & Departament de Matemàtica Aplicada I,
Universitat Politècnica de Catalunya, E.T.S.E.I.B., Diagonal 647, 08028 Barcelona, Spain

The aim of this paper is to provide the state of the art on libration point orbits. We will focus in the Dynamical Systems approach to the problem, since we believe that it provides the most global picture and, at the same time, allows to do the best choice of both strategy and parameters in several mission analysis aspects.

I. Dynamics and phase space around the Libration Points

1. Equations of motion and Libration Points

1.1. *The Restricted Three Body Problem and its perturbations*

It is well known that several very simple models, such as the Two Body Problem or the Restricted Three Body Problem (RTBP), are suitable for spacecraft mission design, since they give good insight of the dynamics in many real situations. In this section we will review some of the most

relevant restricted models for the analysis of the motion in the vicinity of the libration points.

Most of the well known restricted problems take as starting point the circular RTBP, that models the motion of a massless particle under the gravitational attraction of two punctual primaries revolving in circular orbits around their center of mass. In a suitable coordinate system and with adequate units, the Hamiltonian of the RTBP is (Szebehely [70])

$$H(x,y,z,p_x,p_y,p_z) = \frac{1}{2}(p_x^2+p_y^2+p_z^2) + yp_x - xp_y \\ - \frac{1-\mu}{((x-\mu)^2+y^2+z^2)^{1/2}} - \frac{\mu}{((x-\mu+1)^2+y^2+z^2)^{1/2}},$$

being $\mu = m_2/(m_1+m_2)$, where $m_1 > m_2$ are the masses of the primaries. In order to get closer to more realistic situations, or simplifications, this model is modified in different ways. For instance,

(1) Hill's problem. Is useful for the analysis of the motion around m_2. Can be obtained setting the origin at m_2, rescaling coordinates by a factor $\mu^{1/3}$ and keeping only the dominant terms of the expanded Hamiltonian in powers of $\mu^{1/3}$. The Hamiltonian function is

$$H = \frac{1}{2}(p_x^2+p_y^2+p_z^2) + yp_x - xp_y - \frac{1}{(x^2+y^2+z^2)^{1/2}} - x^2 + \frac{1}{2}(y^2+z^2).$$

This Hamiltonian corresponds to a Kepler problem perturbed by the Coriolis force and the action of the Sun up to zeroth-order in $\mu^{1/3}$. Hill's model is the appropiate first approximation of the RTBP for studying the neighborhood of m_2 which takes into consideration the action of the primary m_1 (Simó & Stuchi [68]). This model has a remarcable set of solutions known as the *Variation Orbit Family*. This is a family of $2\pi m$–periodic solutions (m is the parameter of the family) which serves as the first approximation in the modern theory of lunar motion.

(2) Restricted Hill four body problem. This is a time–periodic model that contains two parameters: the mass ratio μ of the RTBP and the period parameter m of the Hill Variation Orbit. The RTBP is recovered as $m \to 0$, and the classical Hill model is recovered as $\mu \to 0$, both in the proper reference frames (Scheeres [60]).

(3) The elliptic RTBP. It is a non–autonomous time–periodic perturbation of the RTBP in which the primaries move in an elliptic orbit instead of a circular one (Szebehely [70]).

(4) The Bicircular Restricted Problem. Is one of the simplest restricted problems of four bodies, obtained from the RTBP by adding a third primary. It can be also considered a periodic perturbation of the the RTBP in which one primary has been splitted in two that move around their common center of mass. This model is suitable to take into account the gravitational effect of the Sun in the Earth–Moon RTBP or the effect of the Moon in the Sun–Earth RTBP. In a coordinate system revolving with Earth and Moon, the Hamiltonian of this problem is (see Simó *et al.* [65])

$$\begin{aligned} H = {} & \frac{1}{2}(p_x^2 + p_y^2 + p_z^2) + yp_x - xp_y \\ & - \frac{1-\mu}{((x-\mu)^2 + y^2 + z^2)^{1/2}} - \frac{\mu}{((x-\mu+1)^2 + y^2 + z^2)^{1/2}} \\ & - \frac{m_S}{((x - a_S\cos\theta)^2 + (y + a_S\sin\theta)^2 + z^2)^{1/2}} - \frac{m_S}{a_S^2}(y\sin\theta - x\cos\theta), \end{aligned}$$

with $\theta = w_S t + \theta_0$, where w_S is the mean angular velocity of the Sun, m_S its mass and a_S the distance from the Earth–Moon barycenter to the Sun.

(5) Coherent models. They are restricted four body problems in which the three primaries move along a true solution of the three body problem. These models have been introduced for the study of the motion around the geometrically defined collinear and triangular equilibrium points of the Earth–Moon system (Andreu [1], Howell *et al.* [40]) and the Sun–Jupiter system perturbed by Saturn (Gabern and Jorba [19]). The Hamiltonian of these problems can be written as

$$\begin{aligned} H = {} & \frac{1}{2}\alpha_1(p_x^2 + p_y^2 + p_z^2) + \alpha_2(yp_x - xp_y) \\ & + \alpha_3(xp_x + yp_y + zp_z) + \alpha_4 x + \alpha_5 y \\ & - \alpha_6\left(\frac{1-\mu}{((x-\mu)^2 + y^2 + z^2)^{1/2}} + \frac{\mu}{((x-\mu+1)^2 + y^2 + z^2)^{1/2}}\right. \\ & \left. + \frac{m_S}{((x-\alpha_7)^2 + (y-\alpha_8)^2 + z^2)^{1/2}}\right), \end{aligned}$$

where the α_i are time–periodic functions, with the same basic frequency as the Bicircular Problem.

In a different approach, instead of taking as starting equations those of the RTBP, we can consider Newton's equations for the motion of an in-

finitesimal body in the force field created by the bodies of the Solar System

$$\mathbf{R}'' = G\sum_i m_i \frac{\mathbf{R}_i - \mathbf{R}}{\|\mathbf{R} - \mathbf{R}_i\|^3}.$$

Performing a suitable change of coordinates (see Gómez *et al.* [26,32]), the above equations can be written in Hamiltonian form with the following Hamiltonian function

$$\begin{aligned} H = {} & \beta_1(p_x^2 + p_y^2 + p_z^2) + \beta_2(xp_x + yp_y + zp_z) + \beta_3(yp_x - xp_y) + \\ & + \beta_4(zp_y - yp_z) + \beta_5 x^2 + \beta_6 y^2 + \beta_7 z^2 + \beta_8 xz + \\ & + \beta_9 p_x + \beta_{10} p_y + \beta_{11} p_z + \beta_{12} x + \beta_{13} y + \beta_{14} z + \\ & + \beta_{15}\Bigg(\frac{1-\mu}{[(x-\mu)^2 + y^2 + z^2]^{1/2}} + \frac{\mu}{[(x-\mu+1)^2 + y^2 + z^2]^{1/2}} + \\ & \quad + \sum_{i \in \mathcal{S}^*} \frac{\mu_i}{[(x-x_i)^2 + (y-y_i)^2 + (z-z_i)^2]^{1/2}} \Bigg), \end{aligned}$$

where $\mathcal{S}^*$ denotes the set of bodies of the Solar System except the two selected as primaries, and the β_i are time dependent functions that can be computed in terms of the positions, velocities, accelerations and overaccelerations of the two primaries. Notice that this Hamiltonian is, formally, a perturbation of the RTBP one. Most of all the intermediate models that have been mentioned are particular cases of this one. Once two primaries have been selected, a Fourier analysis of the β_i functions (Gómez *et al.* [32]) allows the explicit construction of a graded set of models with an increasing number of frequencies, that can be considered between the RTBP and the true equations.

1.2. *Libration Points and dynamical substitutes*

As it is well known, the RTBP has five equilibrium points: three (L_1, L_2, L_3) are collinear with the primaries and the other two (L_4 and L_5) form an equilateral triangle with them. Although the models introduced in the preceding section are close to the RTBP, all of them, except Hill's model, are non autonomous, so they do not have any critical point. If the model is time–periodic, under very general non–resonance conditions between the natural modes around the equilibrium points and the perturbing frequency, the libration points can be continued to periodic orbits of the model. In the continuation process, the periodic orbit can go through bifurcations to end up in more than a single periodic orbit or reach a turning point

and dissapear. These periodic orbits, which have the same period as the perturbation, are the dynamical substitutes of the equilibrium points. For models with a quasi–periodic perturbation the corresponding substitutes will be also quasi–periodic solutions (see Figure 1).

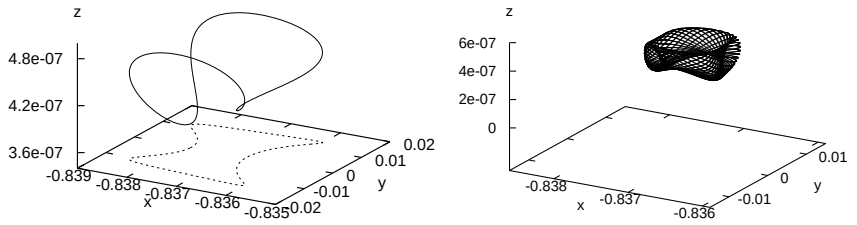

Fig. 1. Dynamical substitutes for the L_1 point in the Earth–Moon system for a time–periodic (left) and a quasi–periodic (right) model.

Dynamical substitutes of the triangular points, for several of the models already mentioned, have been studied in Gómez *et al.* [24], Simó et al. [65] and Jorba *et al.* [44]. For the collinear points of the Sun–Earth system, the dynamical substitutes of L_2 for time–periodic models have been given by Farquhar [17], Howell [40]. Andreu [1] does a complete study of the substitutes of the collinear libration points for a coherent model close to the Earth–Moon problem and compares some of the results obtained with the ones corresponding to a bicircular model. For models depending in more than one frequency one can find results in these Proceedings.

2. The phase space about the Libration Points

In this section we will describe the dynamics near the collinear equilibrium points L_1, L_2, always in the framework of the RTBP. Since we are interested in the motion in the vicinity of a given libration point, following Richardson [58], we set the origin of coordinates at a given libration point and scale variables in such a way that the distance from the smallest primary to the selected equilibrium point will be equal to one. Expanding $r_1 = ((x-\mu)^2 + y^2 + z^2)^{1/2}$ and $r_2 = ((x-\mu+1)^2 + y^2 + z^2)^{1/2}$ in power

series, one gets

$$H = \frac{1}{2}\left(p_x^2 + p_y^2 + p_z^2\right) + yp_x - xp_y - \sum_{n\geq 2} c_n(\mu)\rho^n P_n\left(\frac{x}{\rho}\right), \qquad (1)$$

where $\rho^2 = x^2 + y^2 + z^2$, the c_n are constants depending on the equilibrium point and the mass ratio μ, and P_n is the Legendre polynomial of degree n. With a linear symplectic change of coordinates (Gómez *et al.* [23]), the second order part of the Hamiltonian is set into its real normal form,

$$H_2 = \lambda x p_x + \frac{\omega_p}{2}(y^2 + p_y^2) + \frac{\omega_v}{2}(z^2 + p_z^2),$$

where, for simplicity, we have kept the same notation for the variables. Here, λ, ω_p and ω_v are positive real numbers. From H_2, it is clear that the linear behaviour near the collinear equilibrium points is of the type **saddle** $\times$ **centre** $\times$ **centre**. Hence, one can expect families of periodic orbits which in the limit have frequencies related to both centers: ω_p and ω_v (called planar and vertical frequencies, respectively). This is assured by the Lyapunov center theorem, unless one of the frequencies is an integer multiple of the other (which only happens for a countable set of values of the mass ratio (see Siegel and Moser [62])). Near the libration points we can also expect 2D tori, with two basic frequencies which tend to ω_p and ω_v when the amplitudes tend to zero. The rigorous existence of these tori is more problematic. First, the basic frequencies at the collinear point can be too close to resonant. Furthermore, the frequencies change with their amplitudes and so, they go across resonances when the amplitudes are changed. This leads to a Cantor set of tori. The proof of the existence of these tori follows similar lines to the proof of the KAM theorem (see Jorba and Villanueva [46]).

Close to the L_1 and L_2 libration points, the dynamics is that of a strong unstable equilibrium, because of the saddle component of the linear approximation. This is the reason why is not feasible to perform a direct numerical simulation of the Poincaré map in order to get an idea of the phase space. Due to the **center** $\times$ **center** part, and when we consider all the energy levels, there are 4D center manifolds around them (they are also called neutrally stable manifolds). On a given energy level this is just a 3D set where dynamics have a "neutral behavior". On it there are periodic orbits and 2D invariant tori. The L_3 point has the same linear behavior, however the instability is quite mild. Nevertheless, the long term effects associated to the unstable/stable manifolds of L_3 or to the ones of the central manifold

around L_3 are extremely important (see Gómez *et al.* [24,26]). In this section we will show results about the phase space in a large neighbourhood of the collinear libration points and will see how all the mentioned invariant sets (periodic orbits and tori) are organized.

2.1. *Local (semi–analytical) approach*

The analysis of the dynamics in the center manifold for values of the energy close to the one of the equilibrium point can be done in a semi–analytical way using different strategies. One consists in performing a reduction of the Hamiltonian that decreases the number of degrees of freedom, removes the hyperbolic directions and allows the numerical study of the Poincaré map in a vicinity of the equilibrium points (see Gómez *et al.* [23] and Jorba and Masdemont [45]). This approach is usually known as the reduction to the center manifold. Note that, generically, the expansions required for these computations cannot be convergent in any open set, because of the crossing of resonances. Another procedure consists in the use of Lindstedt-Poincaré methods to explicitly compute the periodic orbits the invariant tori (see Richardson [57] and Gómez et al. [23,26,33]). It looks for analytical expressions for them in terms of suitable amplitudes and phases. Both approaches are limited by the convergence of the expansions used for the changes of coordinates and the Hamiltonian, in the first case, and for the periodic orbits and invariant tori, in the second one, which is discussed in the mentioned papers. The general ideas and main results obtained with both procedures will be discussed in the next two sections.

Reduction to the center manifold

The reduction to the center manifold is similar to a normal form computation. The objective is to remove not all the monomials in the expansion H (up to a given order) but to remove only some, in order to have an invariant manifold tangent to the elliptic directions of H_2. This is done through a series of changes of variables which can be implemented by means of the Lie series method (Deprit [12]).

The Hamiltonian of the RTBP, with the second order terms in normal

form, can be written, in a suitable set of coordinates and momenta, as

$$H(q,p) = \sqrt{-1}\omega_v q_1 p_1 + \sqrt{-1}\omega_p q_2 p_2 + \lambda q_3 p_3 + \sum_{n\geq 3} H_n(q,p), \tag{2}$$

where H_n denotes an homogeneous polynomial of degree n.

To remove the instability associated with the hyperbolic character of H, we first note that, in the second order part of the Hamiltonian, H_2, the instability is given by the term $\lambda q_3 p_3$. Thus, in the linear approximation of the equations of motion, the central part is obtained setting $q_3 = p_3 = 0$. If we want the trajectory to remain tangent to this space when adding the nonlinear terms, this is, with $q_3(t) = p_3(t) = 0$ for all $t > 0$ once we set $q_3(0) = p_3(0) = 0$, we need to have $\dot{q}_3(0) = \dot{p}_3(0) = 0$. Then, because of the autonomous character of the system, we will obtain $q_3(t) = p_3(t) = 0$ for all $t \geq 0$.

Recalling the form of the Hamiltonian equations of motion, $\dot{q}_i = H_{p_i}$, $\dot{p}_i = -H_{q_i}$, one can get the required condition, $\dot{q}_3(0) = \dot{p}_3(0) = 0$ for $q_3(0) = p_3(0) = 0$, when, in the series expansion of the Hamiltonian, H, all the monomials $h_{ij} q^i p^j$ with $i_3 + j_3 = 1$ have $h_{ij} = 0$ (i and j stand for (i_1, i_2, i_3) and (j_1, j_2, j_3), respectively). This happens if there are no monomials with $i_3 + j_3 = 1$. Of course, other expansions could give us the same required tangency condition, but this is the one that needs to cancel less monomials in (2) and, in principle, it is better behaved both in terms of convergence and from a numerical point of view.

All the computations can be implemented using specific symbolic manipulators that can carry out the full procedure up to an arbitrary order (see Jorba [45]). In this way, we end up with a Hamiltonian $H(q,p) = H_N(q,p) + R_N(q,p)$, where $H_N(q,p)$ is a polynomial of degree N in (q,p) without terms with $i_3 + j_3 = 1$, and $R_N(q,p)$ is a remainder of order $N+1$ that is skipped in the computations.

In order to reduce the number of degrees of freedom, after setting $q_3 = p_3 = 0$ in the initial conditions we look only for orbits in the same energy level; in this way only three free variables remain. A further reduction is obtained by looking not at the full orbits, but just at their crossings of a surface of section. Now, all the libration orbits with a fixed Hamiltonian value can be obtained just varying two variables in the initial conditions. For instance, the initial conditions can be chosen selecting arbitrary values for

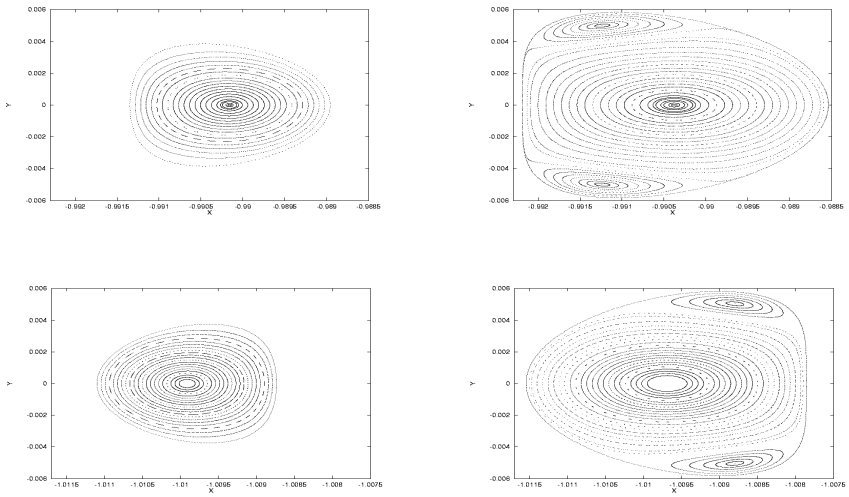

Fig. 2. Poincaré maps on the section $z = 0$ (in RTBP coordinates) of the orbits in the central manifold of L_1 (two top figures) and L_2 (two bottom figures) for the following values of the Jacobi constant: 3.00085, and 3.00078515837634. RTBP mass parameter of the Earth+Moon–Sun system, $\mu = 3.040423398444176 \times 10^{-6}$.

q_2 and p_2, setting $q_1 = 0$ (the surface of section), and finally computing p_1 in order to be in the selected level of Hamiltonian energy. The propagation of this initial condition, looking when and where it crosses the surface of section again and again, gives what is called the images of the Poincaré map on the Poincaré section $q_1 = 0$. Alternatively, the plane $z = 0$ (in RTBP coordinates) can be used to get a more familiar picture. Note that, due to the linear part of the RTBP equations of motion around the collinear equilibrium points (3), $z = 0$ is a surface of section for all the libration orbits in a neighbourhood of the equilibrium point except for the planar ones, which are contained in the $z = 0$ plane.

This is the procedure used to get Figure 2, where the libration orbits around L_1 and L_2 are displayed for two different values of the Jacobi constant, C_J, of the RTBP. From Figure 2, we note that for each level of C_J there is a bounded region in the Poincaré section. The boundary of the region is the planar Lyapunov orbit of the selected energy (related to the planar frequency ω_p of H_2), and is completely contained in the surface of

section. The fixed point, in the central part of the figures, corresponds to an almost vertical periodic orbit, related to the vertical frequency ω_v. Surrounding the central fixed point, we have invariant curves corresponding to Lissajous orbits. The motion in this region is essentially quasi-periodic (except for very small chaotic zones that cannot be seen in the pictures).

Depending on the value of the Jacobi constant, there appear two additional fixed points close to the boundary. These points are associated to halo orbits of class I (north) and class II (south). Surrounding the fixed points corresponding to the halo orbits, we have again invariant curves related to quasi-periodic motions. These are Lissajous orbits around the halos that we call quasi-halo orbits (see Gómez *et al.* [33]).

Finally, in the transition zone from central Lissajous to quasi-halo orbits there is an homoclinic connection of the planar Lyapunov orbit. We note that the homoclinic trajectory that goes out from the orbit and the one that goes in do not generally coincide; they intersect with a very small angle. This phenomenon is known as splitting of separatrices. We also note in this case, that the planar Lyapunov orbit is unstable even in the central manifold.

Lindstedt-Poincaré procedures: halo, quasi-halo, and Lissajous orbits

The planar and vertical Lyapunov periodic orbits, as well as the Lissajous, halo, and quasi-halo orbits, can be computed using Lindstedt–Poincaré procedures and ad–hoc algebraic manipulators. In this way one obtains their expansions, in RTBP coordinates, suitable to be used in a friendly way. In this section we will give the main ideas used for their computation.

We will start with the computation of the Lissajous trajectories (2D tori) and halo orbits (1D tori or periodic orbits). The RTBP equations of motion can be written as

$$\begin{aligned} \ddot{x} - 2\dot{y} - (1 + 2c_2)x &= \frac{\partial}{\partial x} \sum_{n\geq 3} c_n \rho^n P_n \left(\frac{x}{\rho}\right), \\ \ddot{y} + 2\dot{x} + (c_2 - 1)y &= \frac{\partial}{\partial y} \sum_{n\geq 3} c_n \rho^n P_n \left(\frac{x}{\rho}\right), \\ \ddot{z} + c_2 z &= \frac{\partial}{\partial z} \sum_{n\geq 3} c_n \rho^n P_n \left(\frac{x}{\rho}\right), \end{aligned} \tag{3}$$

with c_n, ρ and P_n as in (1). The solution of the linear part of these equations is

$$\begin{aligned} x(t) &= \alpha \cos(\omega_p t + \phi_1), \\ y(t) &= \kappa\alpha \sin(\omega_p t + \phi_1), \\ z(t) &= \beta \cos(\omega_v t + \phi_2), \end{aligned} \tag{4}$$

where ω_p and ω_v are the planar and vertical frequencies and κ is a constant. The parameters α and β are the in-plane and out-of-plane amplitudes of the orbit and ϕ_1, ϕ_2 are the phases. These linear solutions are already Lissajous trajectories. When we consider the nonlinear terms, we look for formal series solutions in powers of the amplitudes α and β of the type

$$\begin{Bmatrix} x \\ y \\ z \end{Bmatrix} = \sum_{i,j=1}^{\infty} \left(\sum_{|k|\le i, |m|\le j} \begin{Bmatrix} x \\ y \\ z \end{Bmatrix}_{ijkm} \begin{Bmatrix} \cos \\ \sin \\ \cos \end{Bmatrix} (k\theta_1 + m\theta_2) \right) \alpha^i \beta^j, \tag{5}$$

where $\theta_1 = \omega t + \phi_1$ and $\theta_2 = \nu t + \phi_1$. Due to the presence of nonlinear terms, the frequencies ω and ν cannot be kept equal to ω_p and ω_v, and they must be expanded in powers of the amplitudes

$$\omega = \omega_p + \sum_{i,j=1}^{\infty} \omega_{ij} \alpha^i \beta^j, \quad \nu = \omega_v + \sum_{i,j=1}^{\infty} \nu_{ij} \alpha^i \beta^j.$$

The goal is to compute the coefficients x_{ijkm}, y_{ijkm}, z_{ijkm}, ω_{ij}, and ν_{ij} recurrently up to a finite order $N = i + j$. Identifying the coefficients of the general solution (5) with the ones obtained from the solution of the linear part (4), we see that the non zero values are $x_{1010} = 1$, $y_{1010} = \kappa$, $z_{1010} = 1$, $\omega_{00} = \omega_p$ and $\nu_{00} = \omega_v$. Inserting the linear solution (4) in the equations of motion, we get a remainder for each equation, which is a series in α and β beginning with terms of order $i + j = 2$. In order to get the coefficients of order two, this known order 2 terms must be equated to the unknown order 2 terms of the left hand side of the equations. The general step is similar. It assumes that the solution has been computed up to a certain order $n - 1$. Then it is substituted in the right hand side of the RTBP equations, producing terms of order n in α and β. This known order n terms must be equated with the unknown terms of order n of the left hand side.

The procedure can be implemented up to high orders. In this way we get, close to the equilibrium point, a big set of KAM tori. In fact, between these tori there are very narrow stochastic zones (because the resonances are

dense). Hence we will have divergence everywhere. However, small divisors will show up only at high orders (except the one due to the 1:1 resonance), because at the origin ω_p/ω_v is close to 29/28. The high order resonances have a very small stochastic zone and the effect is only seen after a big time interval.

Halo orbits are periodic orbits which bifurcate from the planar Lyapunov periodic orbits when the in plane and out of plane frequencies are equal. This is a 1:1 resonance that appears as a consequence of the nonlinear terms of the equations and, in contrast with the Lissajous orbits, they do not appear as a solution of the linearized equations. Of course, we have to look for these 1-D invariant tori as series expansion with a single frequency. In order to apply the Lindstedt-Poincaré procedure, following Richardson [57], we modify the equations of motion (3) by adding to the third equation a term like $\Delta \cdot z$, where Δ is a frequency type series

$$\Delta = \sum_{i,j=0}^{\infty} d_{ij} \alpha^i \beta^j,$$

that must verify the condition $\Delta = 0$. We start looking for the (non trivial) librating solutions with frequency ω_p

$$\begin{aligned} x(t) &= \alpha \cos(\omega_p t + \phi_1), \\ y(t) &= \kappa\alpha \sin(\omega_p t + \phi_1), \\ z(t) &= \beta \cos(\omega_p t + \phi_2). \end{aligned} \tag{6}$$

We note that after this step, halo orbits are determined up to order 1, and $\Delta = 0$ is read as $d_{00} = 0$. Halo orbits depend only on one frequency or one amplitude since they are 1-D invariant tori, so we have not two independent amplitudes α and β. The relation between α and β is contained in the condition $\Delta = 0$ which implicitly defines $\alpha = \alpha(\beta)$.

When we consider the full equations, we look for formal expansions in powers of the amplitudes α and β of the type

$$\begin{Bmatrix} x \\ y \\ z \end{Bmatrix} = \sum_{i,j=1}^{\infty} \left(\sum_{|k|\le i+j} \begin{Bmatrix} x \\ y \\ z \end{Bmatrix}_{ijk} \begin{Bmatrix} \cos \\ \sin \\ \cos \end{Bmatrix} (k\theta) \right) \alpha^i \beta^j,$$

where $\theta = \omega t + \phi$ and, as in the case of 2-D invariant tori, the frequency ω must be expanded as $\omega = \sum_{i,j=0}^{\infty} \omega_{ij} \alpha^i \beta^j$. The procedure for the computation of the unknown coefficients x_{ijk}, y_{ijk}, z_{ijk}, ω_{ij} and d_{ij} is similar to the one described for the Lissajous trajectories.

Quasi-halo orbits are quasi-periodic orbits (depending on two basic frequencies) on two dimensional tori around a halo orbit. Given a halo orbit of frequency ω, the series expansions for the coordinates of the quasi-halo orbits around it will be of the form

$$\left\{\begin{array}{c} x \\ y \\ z \end{array}\right\} = \sum_{i=1}^{\infty} \left(\sum_{|k|<i,|m|<i} \left\{\begin{array}{c} x \\ y \\ z \end{array}\right\}_i^{km} \left\{\begin{array}{c} \cos \\ \sin \\ \cos \end{array}\right\} (k(\omega t + \phi_1) + m(\nu t + \phi_2)) \right) \gamma^i.$$

These expansions depend on two frequencies (ω, ν) and one amplitude, γ (related to the size of the torus around the halo orbit). The frequency ν is the second natural frequency of the torus, and it is close to the normal frequency around the base halo orbit. The amplitude, γ, is related to the size of the torus around the "base" halo orbit which is taken as backbone.

In order to apply the Lindstedt-Poincaré method to compute the quasi-halo orbits, it is convenient to perform a change of variables transforming the halo orbit to an equilibrium point of the equations of motion. Then, orbits librating around the equilibrium point in the new coordinates correspond to orbits librating around the halo orbit in the original ones. The details of the procedure for their computation can be found in Gómez *et al.* [33].

In Figure 2 we display a sample of the different kind of orbits computed using the Lindsted-Poincaré procedure according to the previous explanations.

2.2. *Numerical approach*

In this section we will show how, with a numerical approach, the analysis of the phase space using semi-analytical methods, can be extended to a wider range of energy values, including several bifurcations and also to the L_3 libration point. The approach is based in the computation of the families of periodic orbits and 2D invariant tori of the center manifolds of the three collinear libration points.

Numerical methods have been widely used to compute fixed points and periodic orbits and we will nor enter into the details for their computation here. The reader can find an excellent exposition in the paper by Doedel *et al.* [13]. There are not many papers dealing with the numerical computation

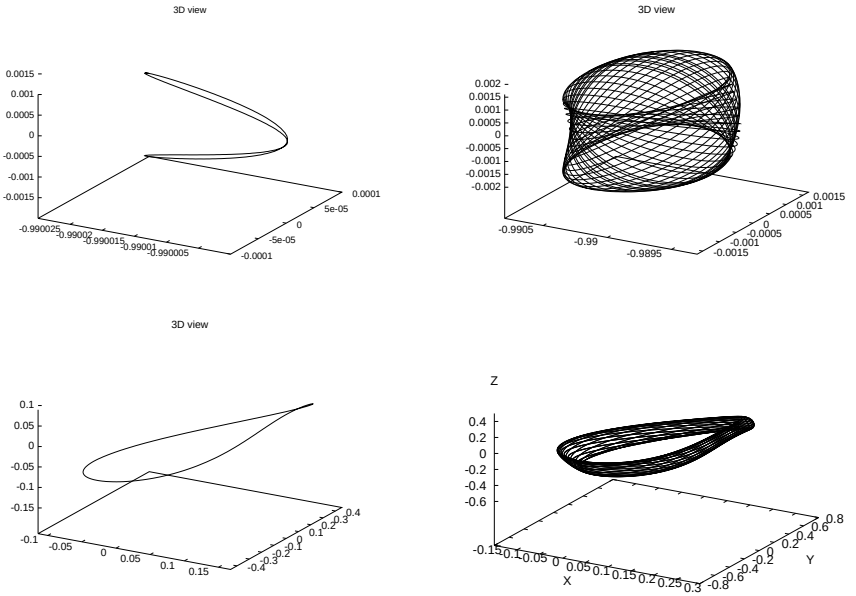

Fig. 3. 3D representation of several types of orbits around L_1. Upper left: vertical periodic orbit with $\alpha = 0.0$ and $\beta = 0.1$ (obtained as a Lissajous orbit with $\alpha = 0$). Upper right: Lissajous orbit with $\alpha = 0.05$ and $\beta = 0.15$. Lower left: halo orbit with $\beta = 0.1$. Lower right: quasi-halo orbit with $\beta = 0.2$ and $\gamma = 0.067$.

of invariant tori. For this purpose, there are mainly two different methods: one is based in looking for a torus as a fixed point of a power of the Poincaré map, P^x, with x being a real number and where P^x is obtained by interpolation. The details of the method, as well as some numerical examples, can be found in Simó [63]. The second procedure, introduced in Castellà and Jorba [8], is based on looking for the Fourier series of the parametrization of an invariant curve on a torus, asking numerically for quasi-periodic motion. This has been the approach, combined with a multiple shooting procedure, that we have used to study the quasi–periodic motions in a neighbourhood of the collinear libration points (Mondelo [55], Gómez *et al.* [34]).

As a first step of the numerical approach, the study of the families of periodic orbits around the libration points and their normal behavior must be done.

Normal behavior around a periodic orbit

Let $\varphi_t(\mathbf{x})$ be the flow of the RTBP. The normal behavior of a T–periodic orbit through $\mathbf{x}_0$ is studied in terms of the time–T flow around $\mathbf{x}_0$, whose linear approximation is given by the monodromy matrix $M = D\varphi_T(\mathbf{x}_0)$ of the periodic orbit. As the monodromy matrix M is symplectic, we have that

$$\operatorname{Spec} M = \{1, 1, \lambda_1, \lambda_1^{-1}, \lambda_2, \lambda_2^{-1}\}.$$

The stability parameters of the periodic orbit, that are defined as $s_j = \lambda_j + \lambda_j^{-1}$ for $j = 1, 2$, can be of one of the following kinds:

- *Hyperbolic*: $s_j \in \mathbb{R}$, $|s_j| > 2$. It is equivalent to $\lambda_j \in \mathbb{R}\backslash\{-1, 1\}$.
- *Elliptic*: $s_j \in \mathbb{R}$, $|s_j| < 2$. It is equivalent to $\lambda_j = e^{i\rho}$ with $\rho \in \mathbb{R}$ (if $|s_j| = 2$, then it is said to be *parabolic*).
- *Complex unstable*: $s_j \in \mathbb{C}\backslash\mathbb{R}$. It is equivalent to $\lambda_j \in \mathbb{C}\backslash\mathbb{R}$, $|\lambda_j| \neq 1$.

If s_j is complex unstable, then s_{3-j} is also complex unstable and, in fact, $s_{3-j} = \overline{s_j}$. After the complex unstable bifurcation, following a Hamiltonian Hopf pattern, there appear invariant tori, as is shown in Pacha [56]. If s_j is hyperbolic, then the periodic orbit has stable and unstable manifolds, whose sections at $\mathbf{x}_0$ through the $\{\lambda_j, \lambda_j^{-1}\}$–eigenplane of M are tangent to the $\{\lambda_j, \lambda_j^{-1}\}$–eigenvectors at $\mathbf{x}_0$. If s_j is elliptic, the $\{\lambda_j, \lambda_j^{-1}\}$–eigenplane of M through $\mathbf{x}_0$ is foliated (in the linear approximation) by invariant curves of the restriction to this eigenplane of the linearization of φ_T (that is, the map $\mathbf{x} \to \mathbf{x}_0 + M(\mathbf{x} - \mathbf{x}_0)$), which have rotation number ρ. For the full system, some of these invariant curves subsist and give rise to 2D tori.

In what follows, we will say that a periodic orbit has central part if one of the stability parameters s_1, s_2 is elliptic. The tori of the central manifolds will be computed starting from the central part of such orbits.

Numerical computation of invarian tori

We look for a parametrization of a 2-dimensional torus $\psi : \mathbb{T}^2 = \mathbb{R}^2/2\pi\mathbb{Z} \to \mathbb{R}^6$, satisfying

$$\psi(\theta + \omega t) = \varphi_t\big(\psi(\theta)\big), \qquad \forall \theta \in \mathbb{T}^2,\ \forall t \in \mathbb{R}, \tag{7}$$

where $\omega = (\omega_1, \omega_2) \in \mathbb{R}^2$ are the frequencies of the torus and $\varphi_t(\mathbf{x})$ is the flow associated to the RTBP. Let us denote by T_i the period corresponding

to the ω_i frequency, that is $T_i = 2\pi/\omega_i$, and $\theta = (\xi, \eta)$. In order to reduce the dimension of the problem, instead of looking for the parametrization of the whole torus, we can look for the parametrization of a curve $\{\eta = \eta_0\}$ (or $\{\xi = \xi_0\}$) on the torus, which is invariant under φ_{T_2}, namely

$$\varphi_{T_2}\big(\psi(\xi, \eta_0)\big) = \psi(\xi + \omega_1 T_2, \eta_0), \qquad \forall \xi \in \mathbb{T}^1. \tag{8}$$

Then, we look for a parametrization $\varphi : \mathbb{T}^1 \to \mathbb{R}^n$ satisfying

$$\varphi(\xi + \rho) = \phi_\delta\big(\varphi(\xi)\big), \qquad \forall \xi \in \mathbb{T}^1, \tag{9}$$

where $\delta = T_2$ and $\rho = \delta\omega_1$. Note that ρ is the rotation number of the curve we are looking for. We assume for φ a truncated Fourier series representation

$$\varphi(\xi) = A_0 + \sum_{k=1}^{N_f} \big(A_k \cos(k\xi) + B_k \sin(k\xi)\big), \tag{10}$$

with A_k, $B_k \in \mathbb{R}^n$. This representation of the geometrical torus $\{\psi(\theta)\}_{\theta \in \mathbb{T}^2}$ is non unique for two reasons: (1) For each choice of η_0 we have a different φ in (10), i.e., a different invariant curve on the torus. (2) Given the parametrization (10), for each $\xi_0 \in \mathbb{T}^1$, $\varphi(\xi - \xi_0)$ is a different parametrization with a different Fourier expansion of the same invariant curve of the torus. In order to overcome both indeterminations, some components of the Fourier coeficients A_k must be fixed.

Finally, and in order to deal with high instabilities, a multiple shooting procedure is used. It consists in looking for several invariant curves on the torus $\{\psi(\theta)\}_{\theta \in \mathbb{T}^d}$ instead of just one, in order to reduce the maximum time of integration to a fraction of δ. Concretely, we will look for m parametrizations $\varphi_0, \varphi_1, \ldots, \varphi_{m-1}$ satisfying for all $\xi \in \mathbb{T}^1$: $\varphi_{j+1}(\xi) = \phi_{\delta/m}\big(\varphi_j(\xi)\big)$, for $j = 0 \div m - 2$ and $\varphi_0(\xi + \rho) = \phi_{\delta/m}\big(\varphi_{m-1}(\xi)\big)$.

The details of the computational aspects (implementation, computing effort, parallel strategies, etc.) of this procedure are given in Gómez *et al.* [34]. As a sample of the tori that can be computed with this procedure, in Fig. 4 we display families around bifurcated halo-type orbits of L_1 and L_2 with central part.

Invariant tori starting around vertical orbits

In Fig. 5 we have displayed the region (in the energy–rotation number plane) covered by the 2–parametric family of tori computed starting from

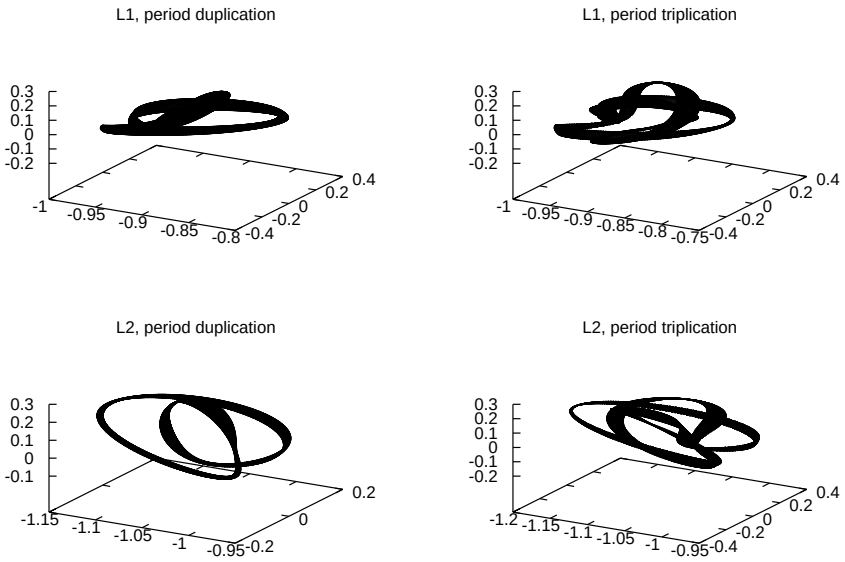

Fig. 4. Tori around the bifurcated halo-type orbits. The two on the top are in the families around L_1 and have energy $h = -1.501$. The two on the bottom are in the families around L_2 and have energy $h = -1.507$.

the vertical L_1 Lyapunov families of periodic orbits with central part. The diagrams corresponding to L_2 and L_3 are similar (see Gómez *et al.* [34]). The boundary has different pieces:

- The lower left piece α (from vertex 1 to 2) is related to the the planar Lyapunov family. The orbits of this family represented in the curve are just the first piece of the family with central part. The horizontal coordinate is the energy level h of the curve and the vertical coordinate is $\rho = (2\pi)^2/(2\pi - \nu) - 2\pi$, where $2\cos\nu$ is the stability parameter of the orbit.
- The upper piece β (from vertex 2 to 3) is strictly related to the vertical Lyapunov family. The points on this curve are (h, ρ) where h is the energy of the orbit and the rotation number ρ is such that the elliptic stability parameter of this orbit is $2\cos\rho$. Note that this relation between ρ and ν is different from the previous item, and this is so in order to have continuity of ρ along an isoenergetic family of tori.
- The bottom boundary γ (from vertex 3 to 1), that corresponds to $\rho = 0$,

begins at the value of the energy where the halo families are born. It is related to a separatrix between the tori around the vertical Lyapunov families and the halo ones.

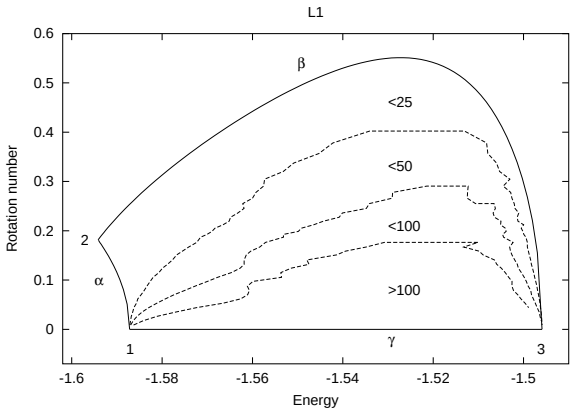

Fig. 5. Region in the energy–rotation number plane, covered by the two-parametric family of tori computed starting at the vertical Lyapunov family of p.o. for L_1. The number of harmonics used for the computation of Fourier representation of the tori (< 25, < 50, < 100 and > 100) is shown in the figure. Vertex 1 is at the value of the energy at which the halo family is born. Vertex 2 is at the value of the energy of the equilibrium point. Vertex 3 is at the value of the energy of the first bifurcation of the vertical Lyapunov family.

There are different ways of computing the tori within the region surrounded by the curves mentioned above. We always start from the pieces of boundary formed by periodic orbits. One possibility is then to perform the continuation procedure keeping fixed the value of the energy h. Another one is to allow variation of the energy but keeping fixed the rotation number ρ. In this last case, and in order to be as close as possible of conditions that guarantee the existence of tori, it is convenient to set the rotation number "as irrational as possible". To this end, when we have used this second strategy, we have set the values of ρ such that $2\pi/\rho$ is an integer plus the golden number. In both cases, and for all L_1, L_2 and L_3 cases, we have always reached a region where the number of harmonics is larger than the maximum value allowed, which at most has been set equal to 100. Larger values of this parameter make computing time prohibitive. Just to have an idea of the computing effort, the constant rotation number family

with $\rho = 0.176$ requires about 3 days of CPU time of an Intel Pentium III at 500MHz.

A "second view" of the center manifold

Using the periodic orbits and the tori computed using the afore mentioned strategies, we have been able to extend the Poincaré map representation of the central manifolds around the collinear libration points. Figures 6 and 7 show the results for L_1, and L_3, respectively (the results for L_2 are close to the ones obatined for L_1). In all these figures we have represented the x–y coordinates at the intersections with $z = 0$, $p_z > 0$. All the plots have a similar structure. The exterior curve in each plot is the Lyapunov planar orbit of the energy level corresponding to the plot. As this orbit is planar, it is completely included in the surface of section, and is the only orbit for which this happens. For the three equilibrium points, and for small energy values, the whole picture is formed by invariant curves surrounding the fixed point associated to the vertical orbit. They are related to the intersections of the Lissajous type trajectories around the vertical periodic orbit. The halo orbits appear at the energy levels corresponding to the first bifurcation of the Lyapunov planar family. This can be seen clearly in the Poincaré map representations, since there appear two additional fixed points surrounded by invariant curves. Increasing the values of the energy, the L_1 and L_2 families of halo orbits have two relevant bifurcations, by period triplication and duplication (see Figure 4). Both bifurcations can be also detected on the Poincaré representations. This additional structure has not been detected for the L_3 case. Within the bifurcated families there are some with central part, which are surrounded by invariant tori. These tori give rise to the typical "island chain" structure of two–dimensional area–preserving maps. This behavior is more clearly seen in a magnification of the figures, as is shown in Gómez et al. [34]. The region between the tori around the vertical Lyapunov orbit and the tori around the halo orbits is not empty, as it appears in the above figures, and should contain, at least, the traces, on the surface of section, of the invariant manifolds of the Lyapunov planar orbit. These manifolds act as separatrices between both kinds of motion. The same thing happens between the islands of the bifurcated halo–type orbits and the tori around the halo orbits. In this case, the region between both kinds of tori is filled with the traces of the invariant manifolds of the bifurcated hyperbolic halo–type orbits. In all these boundary regions, the motion should have a chaotic behavior. With the current tools we have not

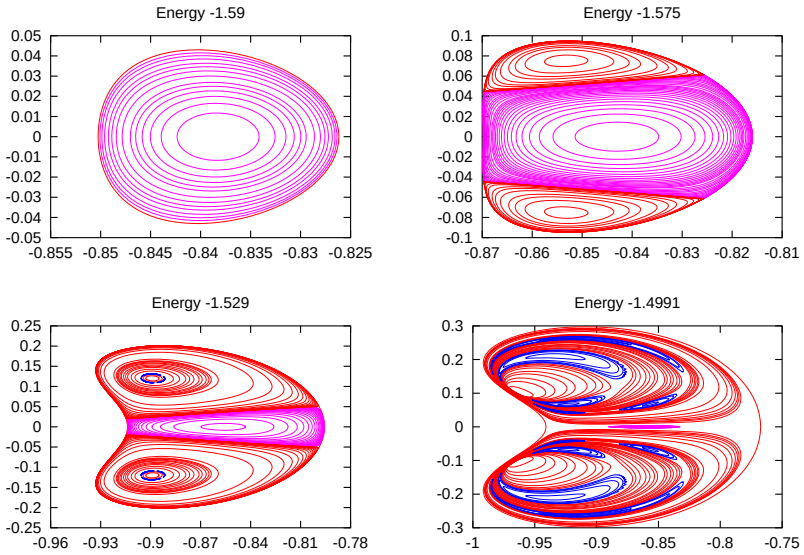

Fig. 6. Energy slices of the section $z = 0$, $p_z > 0$ of the invariant tori around L_1

been able to compute these separatrices.

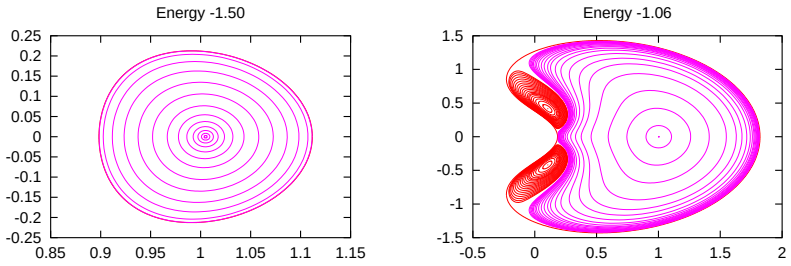

Fig. 7. Energy slices of the section $z = 0$, $p_z > 0$ of the invariant tori around L_3.

3. Computations in very accurate models of motion

The purpose of this section to show procedures to get solutions, close to the ones previously obtained for the RTBP, of more realistic equations of motion as Newton's equations using JPL ephemeris for the motion of the

bodies of the solar system, or some of the intermediate models mentioned in previous sections. For these more realistic models there no complete study of the phase space around the libration points (or their dynamical substitutes) like the one that exists for the RTBP.

Since the solutions will be computed numerically and the equations of motion are time dependent, an initial epoch and a fixed time span is selected and the orbit is computed for this period of time. In the following section we describe a multiple shooting procedure similar to the one used for the numerical solution of boundary-value problems (see Stoer and Bulirsch [69]).

3.1. *Multiple shooting*

As in the standard multiple shooting method, the total time span is splitted into a number of shorter subintervals selecting, for instance, N equally spaced points $t_1, t_2, ..., t_N$. (t_1 is the initial epoch and $t_N - t_1$ the length of the time interval mentioned above). Different time intervals could have also been used. Let us denote $\Delta t = t_{i+1} - t_i$ and by

$$Q_i = (t_i, x_i, y_i, z_i, \dot{x}_i, \dot{y}_i, \dot{z}_i,)^T, \quad i = 1, 2, ..., N$$

the points on a fixed orbit of the RTBP, equally spaced (Δt) in time. This orbit can be, for instance, any of the ones that we have been able to compute their formal expansions using a Lindstedt–Poincaré method. Let $\phi(Q_i)$ be the image of the point Q_i under the flow associated to the equations of motion in the solar system after an amount of time Δt. As, in this way, the epochs t_i are fixed, we can write $Q_i = (x_i, y_i, z_i, \dot{x}_i, \dot{y}_i, \dot{z}_i,)^T$. If all the points Q_i were be on the same orbit of the new equations, we would have $\phi(Q_i) = Q_{i+1}$ for $i = 1, ..., N-1$. Since this is not the case, a change of the starting values is needed in order to fulfill the matching conditions. In this way, one must solve a set of $N-1$ nonlinear equations, which can be written as

$$F \begin{pmatrix} Q_1 \\ Q_2 \\ \vdots \\ Q_N \end{pmatrix} = \begin{pmatrix} \phi(Q_1) \\ \phi(Q_2) \\ \vdots \\ \phi(Q_{N-1}) \end{pmatrix} - \begin{pmatrix} Q_2 \\ Q_3 \\ \vdots \\ Q_N \end{pmatrix} = \Phi \begin{pmatrix} Q_1 \\ Q_2 \\ \vdots \\ Q_{N-1} \end{pmatrix} - \begin{pmatrix} Q_2 \\ Q_3 \\ \vdots \\ Q_N \end{pmatrix} = 0.$$

Newton's method is used to solve the above system. If $Q^{(j)} =$

$\left(Q_1^{(j)}, Q_2^{(j)}, ..., Q_N^{(j)}\right)^T$, denotes the j-th iterate of the procedure, Newton's equations can be written as

$$DF(Q^{(j)}) \cdot (Q^{(j+1)} - Q^{(j)}) = -F(Q^{(j)}),$$

where the differential of the function F has the following structure

$$DF = \begin{pmatrix} A_1 & -I & & \\ & A_2 & -I & \\ & & \ddots & \ddots \\ & & & A_{N-1} \; -I \end{pmatrix},$$

with $D\Phi = \mathrm{diag}(A_1, A_2, ..., A_{N-1})$. As each of the transition matrices, A_i, that appear in $D\Phi$ are 6×6, at each step of the method we have to solve a system of $(N-1) \times 6$ equations with $6 \times N$ unknowns, so some additional conditions must be added. This is the only difference with the standard multiple shooting method and is due to the fact that our problem is not a real boundary-value one. As additional equations we could fix some initial and final conditions at $t = t_0$ and $t = t_N$. In this case one must take care with the choice because the problem can be ill conditioned from the numerical point of view. This is because the matrix $DF(Q)$ can have a very large condition number. To avoid this bad conditioning, we can choose a small value for Δt, but in this case, as the number of points Q_i increases (if we want to cover the same time span), the instability is transfered to the procedure for solving the linear system. Also, the extra boundary conditions can force the solution in a non–natural way giving convergence problems when we try to compute the orbit for a long time interval.

To avoid these problems, we can apply Newton's method directly. As the system has more unknowns than equations, we have (in general) an hyperplane of solutions. From this set of solutions we try to select the one closer to the initial orbit used to start the procedure. This is done by requiring the correction to be minimum with respect to some norm (i.e. the euclidean norm). The use of the normal equations must be avoided because they are usually ill conditioned too. More precisely, denoting by $\Delta Q^{(j)}$

$$\Delta Q^{(j)} = Q^{(j+1)} - Q^{(j)},$$

and requiring $\|\Delta Q^{(j)}\|_2$ to be minimum, one gets the Lagrange function $L(\Delta Q, \mu)$ with (vector) multiplier μ

$$L(\Delta Q, \mu) = \Delta Q^T \cdot \Delta Q + \mu^T \cdot (F(Q) + DF(Q) \cdot \Delta Q).$$

By solving the corresponding Lagrange multipliers problem, we obtain

$$\Delta Q^{(j)} = -DF(Q^{(j)})^T \cdot \left[DF(Q^{(j)}) \cdot DF(Q^{(j)})^T\right]^{-1} \cdot F(Q^{(j)}), \qquad (11)$$

which gives the value of $\Delta Q^{(j)}$ explicitly. However, since the matrix $DF(Q^{(j)})$ is usually very big, a special factorization in blocks is suitable to get the solution 11 in a computationally and efficient way. See Gómez *et al.* [33] for the implementation and the properties of the algorithm.

In order to illustrate the procedure we reproduce the details of some iterations of the computation of a particular solution using JPL ephemeris DE403.

The algorithm is started using as initial nodes, Q_i, that is, the components of $Q^{(0)}$, points on a quasihalo orbit of the Sun–Earth+Moon system around the L_1 point with $\beta = 0.20$ and $\gamma = 0.08$. The initial epoch is fixed to be January 1 2000, and 40 nodes are used with a time step, Δt, between them of 180 days. This covers a total time span of 19.7 years. So, the total number of revolutions "around" the equilibrium point L_1 is approximately 39 and, in order to perform the multiple shooting, approximately one point per revolution has been taken. In Figure 8 we show the (x, y) projection of the orbit after different iterations of the procedure. All the figures are represented in normalized coordinates centered at the L_1 point. The first plot corresponds to the orbit from where the points Q_i were taken, which was computed with the analytical expansions. It is an approximate solution (due to the truncation and asymptotic character of the series) of the RTBP equations of motion. The next two plots, showing large discontinuities at some points, are the results obtained after the first two iterations. The different pieces that constitute the orbit do not match at the nodes in these first steps because the initial conditions were taken from a solution of the RTBP and now we are integrating these initial conditions in a model including all the bodies of the solar system with its real motion. These discontinuities are so large because of the highly unstable character of the solution and because of the small number of nodes per revolution that have been taken. The last plot corresponds to the orbit computed after 8 iterations. The discontinuities that appear in the first iterations are reduced to "zero" by the method. In the first step, adding the corrections applied at all the nodes, the total correction in position $(|\Delta Q^{(0)}_{1,2,3}|_2 + |\Delta Q^{(0)}_{7,8,9}|_2 + ...)$ is of 319600.6 km and of 9360.6 km/day in velocity, which means an average value for the corrections at each point of 8000 km and 235 km/day. After

eight iterations the total amount of the corrections has been reduced to 37 mm and less than 1 mm/day, for positions and velocities, respectively. Taking shorter time intervals between consecutive nodes, the norm of the function F is much smaller at the first steps and the number of Newton iterations decreases. For the Sun–Earth+Moon system, a value of Δt equal to 7 days requires no more than 4 or 5 iterations to get a final solution with discontinuities at the nodes smaller than tracking errors. For the Earth–Moon system, computations must be done more carefully and a time step of half a day usually gives good results.

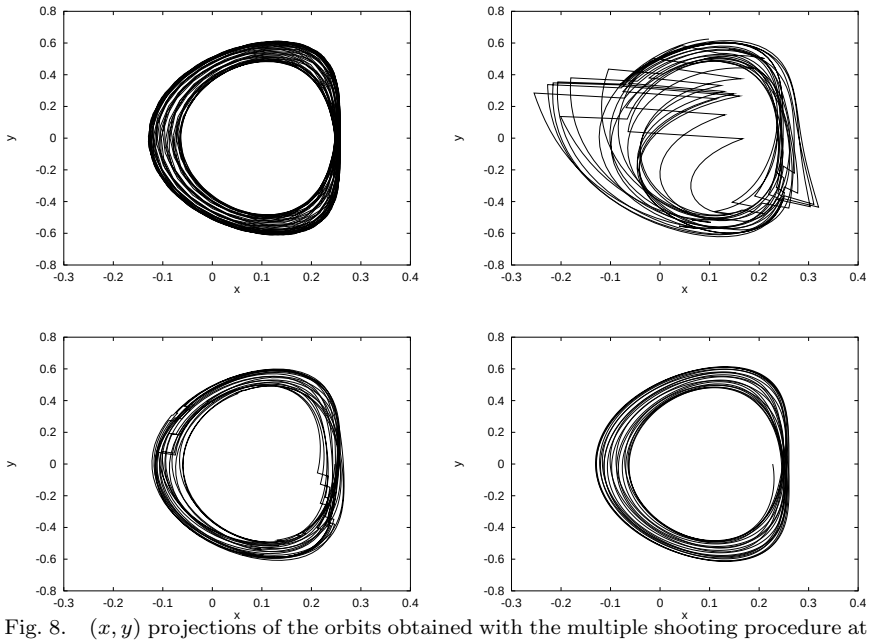

Fig. 8. (x, y) projections of the orbits obtained with the multiple shooting procedure at different steps. The figure on the left upper corner is the orbit of the RTBP, computed from the expansions, from which the initial points Q_i are taken. The orbits with large jumps discontinuities are the ones obtained after the first two iterations. The figure on the right lower corner is the orbit computed after 8 iterations. The initial orbit is a quasihalo orbit with $\beta = 0.2$ and $\gamma = 0.08$.

3.2. *Resonances*

The L_2 point in the Earth–Moon system is quite close to a resonance with solar effects. Because of that, in some sense, the "distance" between the RTBP model and the real one is too large to extend easily the solutions of the RTBP to the real problem.

In order to deal with this situation Andreu [1,2], has introduced a time–dependent restricted four body model that, within a certain degree of simplicity, captures some of the most basic dynamical properties of the true motion around the libration points. The model is time–periodic, since it depends in just one frequency: the difference between the mean sinodical frequencies of the Sun and the Moon. This makes the computation of the most relevant invariant objects of the dynamics simpler.

The main success of the model is that it has allowed the computation of halo-type orbits around L_2 for very large time spans, covering at least a Saros period. When the analytical techniques are applied to get the center manifold around the dynamical substitutes of the libration points, the results allow only the exploration of energy levels very close to the one of he dynamical substitute, so the information obtained is poor.

II. Applications to spacecraft missions

4. Transfer to libration point orbits

4.1. *Transfer using invariant manifolds*

Libration point orbits have, for values of the energy not too far from the ones corresponding to the libration points, a strong hyperbolic character. It is thus possible to use their stable manifolds in order to obtain a transfer. This is what is known in the literature as the dynamical systems approach to the transfer problem. Other ways to obtain transfer trajectories from the Earth to a libration point orbit use optimization procedures. These methods look for orbits between the Earth and the libration orbit maintaining some boundary conditions, subject to some technical constraints, and minimizing the total amount of fuel to be spent in manoeuvres during the transfer

(see Hechler [35]). According to Masdemont [54,21], in the dynamical systems approach one can proceed as follows:

(1) Take a local approximation of the stable manifold at a certain point of the nominal orbit. This dermines a line in the phase space based on a point of the nominal orbit and formed by initial conditions on the stable manifold.
(2) Propagate, backwards in time, the points in the line of the local approximation of the stable manifold until one or several close close approaches to the Earth are found (or up to a maximum time span is reached). In this way some globalization of the stable manifold is obtained.
(3) Look at possible intersections (in configuration space) between the parking orbit of the spacecraft and the stable manifold. At each of these intersections, the velocities in the stable manifold and in the parking orbit have different values, v_s and v_p. A perfect manoeuvre with $\Delta v = v_s - v_p$ would move the spacecraft from the parking orbit to an orbit in the stable manifold that will reach the nominal orbit without any additional manoeuvre.
(4) Then $|\Delta v|$ can be minimized by changing the base point of the nominal orbit at which the stable manifold has been computed (or any equivalent parameter).

Note that, depending on the nominal orbit and on the parking orbit, the intersection described in the third item can be empty, or the optimal solution found in this way can be too expensive. To overcome these difficulties, several strategies can be adopted. One possibility is to perform a transfer to an orbit different from the nominal one and then, with some additional manoeuvres, move to the desired orbits. In a next section we will show how these last kind of transfers can be done. Another possiblility is to allow for some intermediate manoeuvres in the path from the vicinity of the Earth to the final orbit.

In the case in which the nominal orbit is a quasihalo or Lissajous orbit and any phase can be accepted for the additional angular variable, the stable manifold has dimension 3. This produces, on one side, a heavier computational task than in the case of halo orbits, but, on the other side, it gives additional possibilities for the transfer. One should think that the stable manifold of the full center manifold of the collinear libration points

(for a fixed value of t) have dimension 5, which offers a lot of possibilities.

4.2. *The TCM problem*

The Trajectory Correction Manoeuvres (TCM) problem deals with the manoeuvres to be done by a spacecraft in the transfer segment between the parking orbit and the target nominal one. The purpose of the TCMs is to correct the error introduced by the inaccuracies of the injection manoeuvre.

In connection with the Genesis mission (see Lo *et al.* [53]), the TCM problem has been studied in Howell [37] and Serban et al. [61]. For this mission, a halo type orbit around the L_1 point of the Earth–Sun system is used as nominal orbit. The insertion manoeuvre from the parking orbit around the Earth to the transfer trajectory is a large one, with a Δv of the order of 3000 m/s; for the Genesis mission, the error in its execution was expected to be about a 0.2 % of Δv (1 sigma value), and a key point to be studied is how large is the cost of the correction of this error when the execution of the first correction manoeuvre is delayed.

In the paper by Serban *et al.* [61], two different strategies are considered to solve this problem, both of them using an optimization procedure and producing very close results. It is numerically shown that, in practice, the optimal solution can be obtained with just two TCMs and that the cost behaves almost linearly with respect to both the TCM1 epoch and the launch velocity error.

The same results can be obtained without using any optimal control procedure. This is what is done in Gómez *et al.* [28]. The quantitative results, concerning the optimal cost of the transfer and its behaviour as a function of the different free parameters, turn out the same as in Serban *et al.* [61]. Additionally, we provide information on the cost of the transfer when the correction manoeuvres cannot be done at the optimal epochs. These results are qualitatively very close to those obtained in Wison *et al.* [59] for the cost of the transfer to a Lissajous orbit around L_2, when the time of flight between the departure and the injection in the stable manifold is fixed, but the target state (position and velocity) on the manifold is varied. For this problem, it is found that the cost of the transfer can rise dramatically.

In our approach the transfer path is divided in three different legs:

- The first leg goes from the fixed departure point to the point where the TCM1 is performed. Usually, this correction manoeuvre takes place few days after the departure.
- The second leg, between the two trajectory correction manoeuvres TCM1 and TCM2, is used to perform the injection in the stable manifold of the nominal orbit.
- The last path corresponds to a piece of trajectory on the stable manifold. Since both TCM1 and TCM2 are assumed to be done without errors, the spacecraft will reach the nominal halo orbit without any additional impulse.

Let t_1, t_2 and t_3 be the TCM1, TCM2 and arrival epochs, respectively, and Δv_1, Δv_2 the values of the correction manoeuvres at t_1 and t_2. In this way, given the departure state, X_{dep}, and the time t_1, we define $X_1 = \varphi_{t_1}(X_{dep})$, where $\varphi_t(X)$ denotes the image under the flow of the point X after t time units. Then, the transfer condition is stated as

$$\varphi_{t_2-t_1}(X_1 + \Delta v_1) + \Delta v_2 = \varphi_{t_2-t_3}(X_a), \tag{12}$$

where X_a represents the arrival state to the target orbit, which is chosen as $X_a = X_a^h + d \cdot V^s(X_a^h)$ in the linear approximation of the stable manifold based at the point X_a^h. In (12), the term $X_1 + \Delta v_1$ has to be understood as: to the state X_1 (position and velocity) we add Δv_1 to the velocity. Note that, for a given insertion error ϵ (which determines X_{dep}), we have six equality constraints, corresponding to the position and velocity equations (12), and ten parameters: t_1, t_2, t_3, Δv_1, Δv_2 and X_a (given by the parameter along the orbit), which should be chosen in an optimal way within mission constraints.

The sketch of the exploration procedure is the following. To start with, we consider the error of the injection manoeuvre and t_1 fixed. Two types of explorations appear in a natural way: the fixed time of flight transfers, for which t_3 is fixed, and the free time of flight transfers, where t_3 is allowed to vary. In both cases, we start the exploration fixing an initial value for the parameter along the orbit, X_a. In the case of fixed time of flight, the problem then reduces to seven parameters (t_2, Δv_1, Δv_2) and the six constraints (12). Using Δv_1 and Δv_2 to match the constraints (12), the cost of the transfer, $\|\Delta v\| = \|\Delta v_1\| + \|\Delta v_2\|$, is seen as a function of t_2. In the case of free time of flight, $\|\Delta v\|$ is seen as a function of t_2 and t_3, or equivalently, as a function of t_2 and the parameter along the flow, $t_{ws} = t_3 - t_2$.

Once we have explored the dependence of the transfer cost with respect to t_2 and t_3, we study the behavior moving the parameter along the orbit, X_a, and finally, the dependence with respect to the magnitude of the error (which is determined by the launch vehicle) and t_1 (which, due to mission constraints, is enough to vary in a narrow and coarse range).

As an example, Figure 9 shows the results obtained when: the magnitude of the error in the injection manoeuvre is $-3m/s$, the first manoeuvre is delayed 4 days after the departure ($t_1 = 4$), and the total time of flight, t_3, is taken equal to 173.25 days.

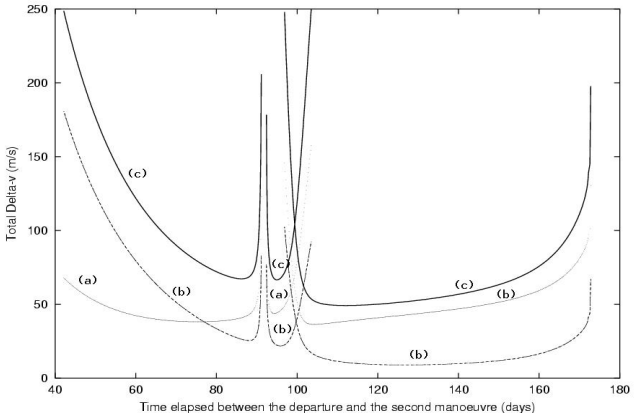

Fig. 9. Cost of the trajectory correction manoeuvres when TCM1 is delayed 4 days after departure and the total time of flight is fixed to 173.25 days. The curves labelled with (a) correspond to $\|\Delta v_1\|$, those with (b) to $\|\Delta v_2\|$ and those with (c) to the total cost: $\|\Delta v_1\| + \|\Delta v_2\|$.

Several remarks should be done in connection with the Figure:

- The solutions of equation (12) are grouped along, at least, three curves. For $t_2 = 99.5$ days there is a double point in the cost function, corresponding to two different possibilities.
- For $t_2 = 113$ days we get the optimum solution in terms of fuel consumption: $\|\Delta v_1\| + \|\Delta v_2\| = 49.31$ m/s. This value is very close to the one given in Serban et al. [61] for the MOI approach, which is 49.1817 m/s. The discrepancies can be attributed to slight differences between the two nominal orbits and the corresponding target points.

- When t_2 is small or very close to the final time, t_3, the total cost of the TCMs increases, as it should be expected.
- Around the values $t_2 = 92$, 97 and 102 days, the total cost increases abruptly. This sudden grow is analogous to the one described in Howell and Barden [37] in connection with the TCM problem for the Genesis mission. It is also similar to the behaviour found in Wilson *et al.* [59] for the cost of the transfer to a Lissajous orbit around L_2, when the time of flight between the departure and the injection in the stable manifold is fixed. This fact can be explained in terms of the angle between the two velocity vectors at $t = t_2$, this is when changing from the second to the third leg of the transfer path. This angle also increases sharply at the corresponding epochs.

5. Transfers between libration point orbits

In this section we will show a method for performing transfers between libration point orbits around the same equilibrium point.

The interest on this problem was initially motivated by the study of the transfer from the vicinity of the Earth to a halo orbit around the equilibrium point L_1 of the Earth-Sun system (Gómez et al. [23,22], Masdemont [54]). There, it was shown that the invariant stable manifolds of halo orbits can be used efficiently for the transfer from the Earth, if we are able to inject the spacecraft into that manifolds. This can be achieved easily when the orbits of the manifold come close to the Earth. But this is true only when the halo orbit is large enough, or when the effect of the Moon, bending some orbits of the manifold, is big enough to take these orbits near the Earth. For small halo orbits, if a swingby with the Moon is used, there are launch possibilities only during two or three days per month (Eismont [14], Gómez et al. [22,21], Masdemont [54]). These launching possibilities can be longer for halo orbits with larger z-amplitude. This is because they have a stable manifold coming closer to the Earth. After the transfer from the Earth to a large halo orbit has been done, we must be able to go from it to a smaller one in a not very expensive way, in terms of the Δv consumption and time. Although this rule also applies for the transfer to Lissajous orbits, the study of the transfer between Lissajous orbits was first motivated by the missions FIRST, Plank and GAIA of the European Space Agency Scientific Program. FIRST is the cornerstone project in the ESA Science Program dedicated

to far infrared Astronomy. Planck, renamed from COBRAS/SAMBA, is to map the microwave background over the whole sky and is now combined with FIRST for a launch in 2007. Several possible options where considered during the orbit analysis work. The final one adopted was the so-called "Carrier", where both spacecrafts will be launched by the same Ariane 5, but will separate after launch. For this option, the optimum solution is a free transfer to a large amplitude Lissajous orbit. FIRST will remain in this orbit, whereas Planck, of much less mass, will perform size reduction manoeuvres.

In what follows we will consider the problem of the transfer between both halo type and Lissajous orbits, always around the same libration point.

5.1. *Transfers between halo orbits*

The method that we present is based on the local study of the motion around halo orbits, and uses of the geometry of the problem in the neighbourhood of an orbit of this kind (Masdemont [54], Gómez *et al.* [29]). The approach is different from the procedure developed by Hiday and Howell [36,41] for the same problem. In their approach, they select departure and arrival states on two arbitrary halo orbits, and take a portion of a Lissajous trajectory as a path connecting these states. At the patch points there are discontinuities in the velocity which must be minimized. The primer vector theory (developed by Lawden [51] for the two body problem) is extended to the RTBP and applied to establish the optimal transfers.

In our approach, we first study the transfer between two halo orbits which are assumed to be very close in the family of halo orbits. With this hypothesis, the linear approximation of the flow in the neighbourhood of the halo orbits, given by the variational equations, is good enough to have a better understanding of the transfer.

Assume that at a given epoch, t_1, we are on a halo orbit, H_1, and that at this point a manoeuvre, $\Delta v^{(1)}$, is performed to go away from the actual orbit. At $t = t_2 > t_1$, a second manoeuvre, $\Delta v^{(2)}$, is executed in order to get into the stable manifold of a nearby halo orbit H_2. Denoting by $\Delta\beta$ the difference between the z-amplitudes of these two orbits, the purpose of an optimal transfer is to perform both manoeuvres in such a way that the

performance function

$$\frac{\Delta\beta}{\|\Delta v^{(1)}\|_2 + \|\Delta v^{(2)}\|_2},$$

will be maximum.

Let φ be, as usual, the flow associated to the differential equations of the RTBP and $\varphi_\tau(y)$ the image of a point $y \in \mathbb{R}^6$ at $t = \tau$, so we can write

$$\varphi_\tau(y+h) = \varphi_\tau(y) + D\varphi_\tau(y)h + O(\mid h \mid^2) = \varphi_\tau(y) + A(\tau)h + O(\mid h \mid^2).$$

Let x_β be the initial point on a halo orbit, H_1, with z-amplitude β, and let us denote $\phi_\tau(\beta) = \varphi_\tau(x_\beta)$. The corresponding points in the phase space at $t = t_1, t_2$, neglecting higher order terms and assuming that the time required to execute the manoeuvre can be also neglected, will be, respectively,

$$\phi_{t_1}(\beta) + \begin{pmatrix} 0 \\ \Delta v^{(1)} \end{pmatrix}, \quad \text{and} \quad \phi_{t_2}(\beta) + A(t_2)A(t_1)^{-1} \begin{pmatrix} 0 \\ \Delta v^{(1)} \end{pmatrix}.$$

At $t = t_2$, the insertion manoeuvre, $\Delta v^{(2)}$, into the stable manifold of the halo orbit of z-amplitude $\beta + \Delta\beta$ is done. So, denoting by $A_{t_1,t_2} = A(t_2)A(t_1)^{-1}$, we must have

$$\phi_{t_2}(\beta(0)) + A_{t_1,t_2} \begin{pmatrix} 0 \\ \Delta v^{(1)} \end{pmatrix} + \begin{pmatrix} 0 \\ \Delta v^{(2)} \end{pmatrix} = \phi_{t_2}(\beta + \Delta\beta) + \gamma_2 e_{2,\beta+\Delta\beta}(t_2) + \gamma_3 e_{3,\beta+\Delta\beta}(t_2),$$

where $e_{2,\beta+\Delta\beta}(t_2)$ and $e_{3,\beta+\Delta\beta}(t_2)$ are the eigenvectors related to the stable direction and to the tangent to the orbit direction, respectively, of the orbit of amplitude $\beta + \Delta\beta$ at $t = t_2$. The first term in the right hand side of the above equation can be written as

$$\phi_{t_2}(\beta + \Delta\beta) = \phi_{t_2}(\beta) + \frac{\partial \phi_{t_2}(\beta)}{\partial \beta}\Delta\beta + O((\Delta\beta)^2).$$

We want to compute the cost of the transfer per unit of z–amplitude, so we set $\Delta\beta = 1$ and the equation to be solved is, after expanding $e_{i,\beta+\Delta\beta}$ by Taylor around β and neglecting higher order terms,

$$A_{t_1,t_2} \begin{pmatrix} 0 \\ \Delta v^{(1)} \end{pmatrix} + \begin{pmatrix} 0 \\ \Delta v^{(2)} \end{pmatrix} = \frac{\partial \phi_{t_2}(\beta)}{\partial \beta} + \gamma_2 e_{2,\beta}(t_2) + \gamma_3 e_{3,\beta}(t_2),$$

from which we can isolate $\Delta v^{(1)}$, $\Delta v^{(2)}$, getting

$$\Delta v^{(1)} = u_{10} + \gamma_2 u_{12} + \gamma_3 u_{13},$$

$$\Delta v^{(2)} = u_{20} + \gamma_2 u_{22} + \gamma_3 u_{23},$$

for suitable u_{ij}. All the magnitudes that appear in these two equations, except the scalars γ_2 and γ_3, are three-dimensional vectors. As $\Delta\beta = 1$ has been fixed, the maxima of the performance function corresponds to the minima of $\|\Delta v^{(1)}\|_2 + \|\Delta v^{(2)}\|_2$. Computing the derivatives of this function with respect to γ_2 and γ_3 and equating them to zero, we get a system of two polynomial equations of degree four in the two variables γ_2 and γ_3, that must be solved for each couple of values t_1, t_2 (which are the only free parameters).

The results of the numerical computations show that for a fixed value of t_1, there are, usually, two values of t_2 at which the performance function has a local maximum (for values of t_1 close to 90^o and 240^o there are three and four maxima). The difference between these two values of t_2 is almost constant and equal to 180^o. That is, after the first manoeuvre has been done, the two optimal possibilities appear separated by a difference of 1/2 of revolution.

The cost of the transfer using the optimal t_2 is almost constant and the variation around the mean value do not exceeds 4%. As an example, if the z-amplitude of the departure orbit is β =0.1, the optimum value is reached using the first maximum for $t_1 = 102^o$ and $t_2 = 197^o$. For these particular values, the cost of the transfer, per unit of $\Delta\beta$, is of 696 m/s. The cost increases with β: for β =0.15, the optimal value is $\Delta v = 742$ m/s ($t_1 = 102^o$, $t_2 = 193^o$) and for β =0.2 $\Delta v = 785$ m/s ($t_1 = 101^o$, $t_2 = 187^o$). It has been found that the variation with β of the optimal value of the cost is almost linear. The value of t_1 for the first manoeuvre is almost constant and equal to 100^o, the corresponding point in the physical space being always very close to the $z = 0$ plane. For very small values of β, the second manoeuvre must be done after $t_2 = 270^o$, but this value decreases quickly and for $\beta \in (0.1, 0.3)$ it is of the order of $t_2 = 190^o$, approximately. That is, one has to wait, typically, 1/4 of revolution after the first manoeuvre, to do the second one.

The transfer computed with the above procedure is not optimal if the initial and final orbits are not close. This is because the solution given by the linear analysis is not good enough when the orbits have very different z-amplitudes. Several possibilities are discussed in Gómez *et al.*[29]. As a final conclusion we can say that the cost of a unitary transfer is of 756 m/s

and the behaviour with the z–amplitude β is almost linear. In this way, the cost of the transfer between two halo orbits of amplitudes β =0.25 and 0.08 is $(0.25 - 0.08)\times$ 756 m/s = 128.5 m/s. In Figure 10 we show the three projections of a transfer trajectory that goes form $\beta = 0.25$ to $\beta = 0.08$

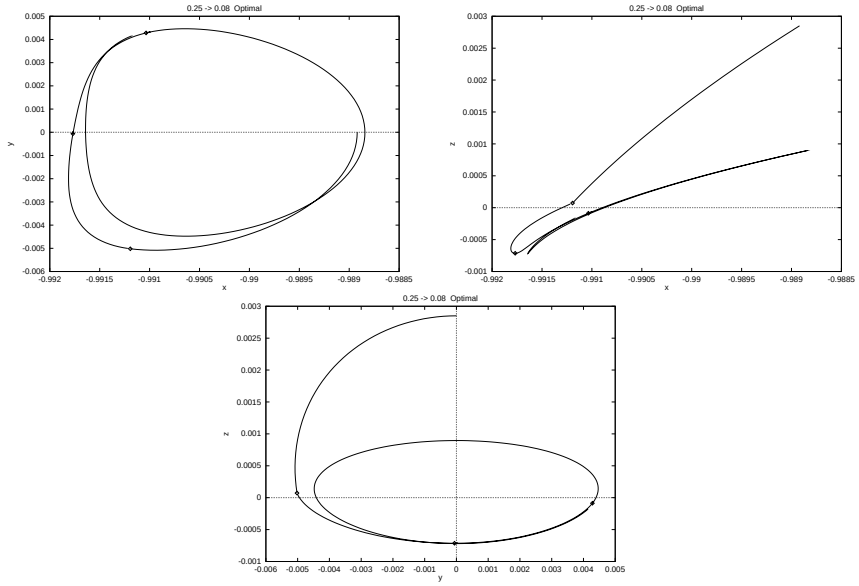

Fig. 10. Projections of the transfer trajectory starting at a departure orbit of z-amplitude $\beta = 0.25$ and arriving at a final one with z-amplitude $\beta = 0.08$. The dotted points correspond to the epochs at which the manoeuvres have been done.

5.2. *Transfers between Lissajous orbits*

The method of this section is based in the dynamical study of the linearized RTBP equations of motion about a collinear equilibrium point. The development was iniciated during preliminary studies of the FIRST/Plank mission (see Cobos and Hechler [9]) and is fully developed in Cobos and Masdemont [10,11].

Let us start with the solution of the linear part of the equations of

motion (3) which can be written as,

$$\left.\begin{aligned} x(t) &= A_1 e^{\lambda t} + A_2 e^{-\lambda t} + A_3 \cos \omega t + A_4 \sin \omega t \\ y(t) &= c A_1 e^{\lambda t} - c A_2 e^{-\lambda t} - \bar{k} A_4 \cos \omega t + \bar{k} A_3 \sin \omega t \\ z(t) &= A_5 \cos \nu t + A_6 \sin \nu t \end{aligned}\right\} \tag{13}$$

where A_i are arbitrary constants and c, $\bar{k}$, ω, λ and ν are constants depending only on c_2.

Introducing amplitudes and phases (13) can also be written as

$$\left.\begin{aligned} x(t) &= A_1 e^{\lambda t} + A_2 e^{-\lambda t} + A_x \cos(\omega t + \phi) \\ y(t) &= c A_1 e^{\lambda t} - c A_2 e^{-\lambda t} + \bar{k} A_x \sin(\omega t + \phi) \\ z(t) &= A_z \cos(\nu t + \psi) \end{aligned}\right\} \tag{14}$$

where the relations are $A_3 = A_x \cos \phi$, $A_4 = -A_x \sin \phi$, $A_5 = A_z \cos \psi$ and $A_6 = -A_z \sin \psi$.

The key point is that, choosing $A_1 = A_2 = 0$, we obtain periodic motions in the xy components with a periodic motion in the z component of a different period. These are the Lissajous orbits in the linearized restricted circular three-body problem, A_x, A_z being the maximum in plane and out of plane amplitudes respectively. The first integrals A_1 and A_2 are directly related to the unstable and stable manifold of the linear Lissajous orbit. For instance, the relation $A_1 = 0, A_2 \neq 0$, defines a stable manifold . Any orbit orbit verifying this condition, will tend forward in time to the Lissajous (or periodic) orbit defined by A_x, A_z, since the A_2-component in (13) will die out. A similar fact happens when $A_1 \neq 0, A_2 = 0$, but now backwards in time. Then, this later condition defines a unstable manifold.

The analysis proceeds by computing the manoeuvres that keep the A_1 component equal to zero in order to prevent escape from the libration zone, and how do the amplitudes change when a manoeuvre is applied. We note that, for the linear problem, the motion in the z-component is uncoupled from the motion in the xy component, and z-manoeuvres only change the A_z amplitude but do not introduce instability. Assume that the motion takes place in a Lissajous orbit with amplitude $A_z^{(i)}$ and phase ψ_i, and that the desired final z-amplitude is $A_z^{(f)}$. The possible z-manoeuvres $\Delta \dot{z}$ wich perform the transfer at time t_m are given by,

$$\frac{\Delta \dot{z}}{\nu} = A_z^{(i)} \sin(\nu t_m + \psi_i) \pm \sqrt{{A_z^{(f)}}^2 - {A_z^{(i)}}^2 \cos^2(\nu t_m + \psi_i)} \tag{15}$$

We note that

- if $A_z^{(f)} \geq A_z^{(i)}$, the transfer manoeuvre is possible at any time, but
- if $A_z^{(f)} < A_z^{(i)}$, the transfer manoeuvre is possible only if the expression inside the square root is possitive; more precisely, when $t \in \left[\varepsilon, \frac{\pi}{\nu} - \varepsilon\right] \cup \left[\frac{\pi}{\nu} + \varepsilon, \frac{2\pi}{\nu} - \varepsilon\right]$, where $\varepsilon = \frac{1}{\nu}(\arccos(\frac{A_z^{(f)}}{A_z^{(i)}}) - \psi_i)$. This condition essentially says that it is not possible to reduce the amplitude with an impulsive manoeuvre in case that the position at time t_m has a z component bigger than $A_z^{(f)}$.

The change in the in-plane amplitude is a little more tricky since one must keep the unstable component equal to zero. Assuming that the motion takes place in a Lissajous orbit with amplitude $A_x^{(i)}$ and phase ϕ_i and the desired final in-plane amplitude is $A_x^{(f)}$, the possible manoeuvres at time t_m are given by

$$(\Delta\dot{x}, \Delta\dot{y}) = \alpha \frac{1}{\sqrt{c^2 + \bar{k}^2}}(d_2, -\bar{k}d_1), \quad \alpha \in \mathbb{R}, \tag{16}$$

where α, indicating the size of the manoeuvre can be

$$\alpha = A_x^{(i)} \sin(\omega t_m + \phi_i - \beta) \pm \sqrt{{A_x^{(f)}}^2 - {A_x^{(i)}}^2 \cos^2(\omega t_m + \phi_i - \beta)},$$

where β is a fixed angle given by the direction of the vector $(c, \bar{k})$. Again we observe that

- if $A_x^{(f)} \geq A_x^{(i)}$, the transfer manoeuvre is possible at any time, but
- if $A_x^{(f)} < A_x^{(i)}$, the transfer manoeuvre is possible only when the expression inside the square root is positive; more precisely, when $t \in \left[\delta, \frac{\pi}{\omega} - \delta\right] \cup \left[\frac{\pi}{\omega} + \delta, \frac{2\pi}{\omega} - \delta\right]$, where $\delta = \frac{1}{\omega}(\arccos(\frac{A_x^{(f)}}{A_x^{(i)}}) - \phi_i + \beta)$.

We also note that the manoeuvre (16) is always in the same direction. This direction plays a similar role to the direction orthogonal to the z-plane in the case of the previously commented z-manoeuvres.

Once the target amplitudes are selected, the epochs of the manoeuvres can be chosen essentially according to the following possibilities:

- Select t_m in order to minimize the Δv expended in changing the amplitude.
- Select t_m in order to reach the target orbit with a selected phase.

Assuming that the amplitudes before and after the manoeuvres are different, in the first case the optimal t_m for changing the in-plane amplitude verifies that the angle $\omega t_m + \phi_i$ equals $\beta + \frac{\pi}{2} + k\pi$, $k \in \mathbb{Z}$. In this case the minimum fuel expenditure for the manoeuvre is $|A_x^{(f)} - A_x^{(i)}|$. In a similar way, the optimal t_m for a change in the out-of-plane amplitude verifies $\nu t_m + \psi_i = \frac{\pi}{2} + k\pi$, $k \in \mathbb{Z}$, and the manoeuvre is given by $\Delta \dot{z} = \nu(A_z^{(f)} - A_z^{(i)})$.

In case that we decide to arrive at the selected Lissajous orbit with a certain phase, the analysis proceeds by considering the in-plane and out-of-plane amplitudes A_x and A_z written in term of its respective components A_3, A_4 and A_5, A_6, and studying the angle which they define. A particular interesting case is the one in which the manoeuvres maintain the amplitudes (the non trivial possibilities of (15) and (16)). In this case, an in-plane manoeuvre (16) at time t_m produces an in-plane change of phase given by

$$\phi_f - \phi_i = -2(\omega t_m - \beta + \phi_i) \qquad (\text{mod } 2\pi), \tag{17}$$

and an out-of-plane manoeuvre (15) produces an out-of-plane change of phase given by

$$\psi_f - \psi_i = -2(\nu t_m + \psi_i) \qquad (\text{mod } 2\pi). \tag{18}$$

These manoeuvres give two strategies for the avoidance of the exclusion zone needed in many missions (see for instance Farquhar [16]). Besides the well known z-strategy given by (18), we have another xy one given by (17), which for the FIRST/Plank mission implies a delta-v expenditure of only 15 m/s every six years (see Cobos and Hechler [9]).

5.3. *Homoclinic and heteroclinic connections*

In the preceding sections, we have shown how to use the local dynamics around a halo orbit for "local" purposes. In this one we will study the global behaviour of the invariant stable/unstable manifolds of the central manifolds of L_1 and L_2, in order to perform some acrobatic motions connecting libration orbits around these equilibrium points.

In order to show some heteroclinic trajectories between libration orbits around L_1 and L_2, we have to match an orbit of the unstable manifold of a libration orbit around one point with another orbit, in the stable manifold of a libration orbit around the other point. This is, both orbits have to be

the same one. Since these orbits, when looked in the X coordinate of the RTBP system, have to go from one side of the Earth to the other one, the place where we look for the connection is the plane $X = \mu - 1$, this is, the plane orthogonal to the X axis that cuts it at the point where the center of the Earth is located.

Although the technical details are much more complex, the main idea is similar to the computations introduced in Gómez *et al.* [27] for $L_{4,5}$ connections. Once a Jacobi constant is fixed, we take initial conditions in the linear approximation of the unstable manifold of all the libration orbits inside the level of energy. Since the energy is fixed, we have three free variables (usually q_1, q_2 and p_2). A scanning procedure in these variables is done. Since the selected orbits will leave the neighbourhood of the libration point, each initial condition in the variables (q, p) is translated into RTBP coordinates and then propagated forward in time until it crosses the plane $X = \mu - 1$. We do the same process for the orbits in the stable manifold, where all the propagation is done backward in time.

We have to remark that, as usual, the unstable and stable manifolds have two branches. In the process we select only the branches that, at the initial steps of the propagations, approach the $X = \mu - 1$ plane.

Since the Jacobi constant is fixed, the set of all RTBP values $\mathcal{C} = \{(Y, \dot{Y}, Z, \dot{Z})\}$ obtained, characterize the branch of the manifold of all the libration orbits around the selected equilibrium point for the particular section. Let us denote these sets like $\mathcal{C}_i^{+sj}$, where $+$ or $-$ denote the branch of the s (stable) or u (unstable) manifold of the L_j, $j = 1, 2$ libration orbits at the i-th intersection with the $X = \mu - 1$ plane.

Looking at the above mentioned branches of the manifolds, the simplest heteroclinic orbits will be obtained from $\mathcal{I}_{1^-} = \mathcal{C}_1^{-s1} \cap \mathcal{C}_1^{-u2}$ and $\mathcal{I}_{1^+} = \mathcal{C}_1^{-u1} \cap \mathcal{C}_1^{-s2}$. Both sets give transfer orbits that cross once the plane $X = \mu - 1$. We will denote by $\mathcal{I}_{k^-}$ (respectively $\mathcal{I}_{k^+}$) the set of heteroclinic trajectories from L_2 to L_1 (resp. from L_1 to L_2) that cross k times the plane $X = \mu - 1$, following the above mentioned branches of the manifold. We note that, due to the symmetries of the RTBP equations, for any heteroclinic orbit from L_1 to L_2 we have a symmetrical one from L_2 to L_1 and so just one exploration must be done.

Unhopefully, it has been found (see Gómez *et al.* [30]) that $\mathcal{I}_{1^+}$ is empty

and so one must look for connections crossing at least twice the plane $X = \mu - 1$. In this case many possibilities of connections appear. As an example, in Figure 11 a connection between a Lissajous orbit around L_2 and a quasi-halo orbit around L_2 is displayed. Both the 3-D representation of the homoclinic orbit and the intersections with the surface of section $Z = 0$, around both equilibrium points, are given.

As another kind of connection, the homoclinic orbit inside the central manifold that marks the transition from the central Lissajous orbits to the quasi-halo ones is computed in Gómez *et al.* [30]. These kind of solutions are interesting because they perform a transition from a planar motion (close to a Lyapunov orbit) to an inclined orbit (close to the quasi-halo orbits) without any Δv. Figure 12 shows one of these orbits in central manifold (q, p) variables. Unfortunately, the transition is very slow but probably, with very small Δv, it could be possible to accelerate the transition from planar to inclined motion.

6. Low energy transfers

According to Simó [64]: "It seems feasible to produce accurate and enough complete descriptions of the dynamics on the center manifolds of the collinear libration points as well as large parts of the corresponding stable and unstable manifolds. Having these concepts in hand, the design of space missions *à la carte*, involving the vicinities of these points, could be done in an automatic way". Although not all the theoretical and practical questions underlying the above idea, and required for its implementation, have been solved, some progress has been done and will be summarized in this section.

The invariant manifold structures associated to the collinear libration points provide not only the framework for the computation of complex spacecraft mission trajectories, but also can be used to understand the geometrical mechanisms of the material transport in the solar system. This has been the approach that has been used recently for the design of low energy transfers from the Earth to the Moon (Koon *et al.* [49]) and for a "Petit Grand Tour" of the Moons of Jupiter (Koon *et al.*[48], Gómez et al. [25]). It has also been used to explain the behaviour of some captured Jupiter comets, see Howell *et al.* [42], Koon et al. [50].

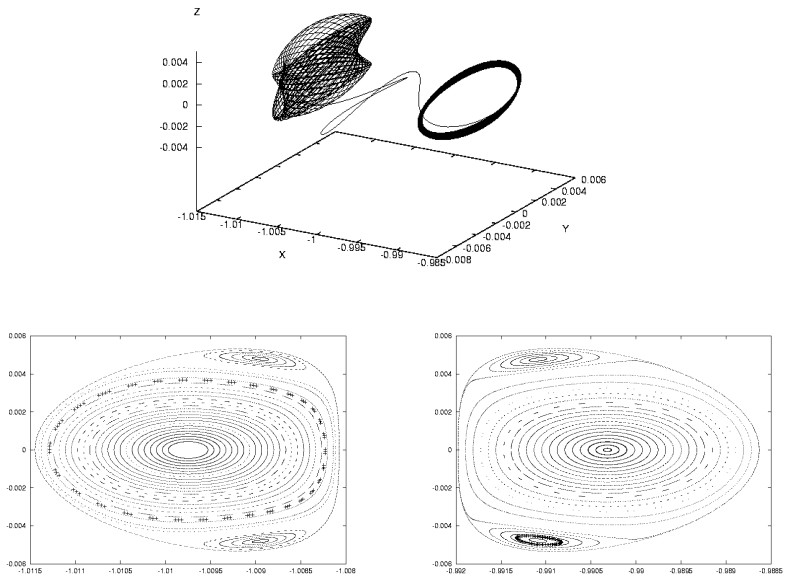

Fig. 11. L_1-L_2 heteroclinic connection between a Lissajous orbit around L_2 and a quasi-halo orbit around L_1. In the lower pictures the intersections of the orbits with the surface of section ($Z = 0$) for L_2 (left) and for L_1 (right) are displayed with crosses.

6.1. *Shoot the Moon*

The goal is to produce transfer orbits from the Earth ending at a lunar capture orbit, using less fuel than in a Hohmann transfer. This problem was first considered by Belbruno and Miller [6] and applied to the Hiten mission in 1991. The present procedure, developed by Koon *et al.* [48], is based in the construction of trajectories with prescribed itineraries and has the following three key steps:

(1) Decouple the Sun–Earth–Moon-Spacecraft system (which is a restricted 4–body problem) in two restricted 3–body problems: the Sun–Earth–Spacecraft and the Earth–Moon-Spacecraft systems.
(2) Use the stable/unstable manifolds of the periodic orbits about the Sun–Earth system L_2 libration points to provide a low energy transfer from

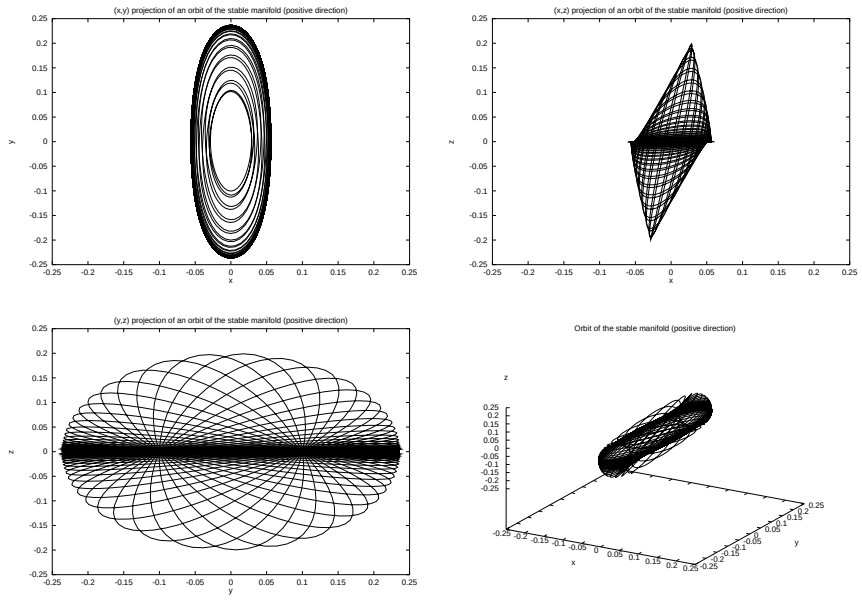

Fig. 12. Homoclinic connection between Lyapunov orbits inside the central manifold (in central manifold coordinates).

the Earth to the stable/unstable manifolds of periodic orbits around the Earth–Moon L_2 libration point. The "low energy" required is needed because some manoeuvres must be done in order to depart slightly from the manifolds and also because the manifold intersection is not a true one, since they are related to different restricted problems.

(3) Finally, use the unstable manifolds of periodic orbits around the Earth–Moon libration points to provide a ballistic capture about the Moon.

In fact, the procedure works as follows: first a suitable Sun–Earth L_2 periodic orbit is computed, as well as their stable and unstable manifolds. Some orbits on the stable manifold come close to the Earth and, at the same time, points close to the unstable manifold propagated backwards in time come close to the stable manifold. So, with an small Δv is possible to go from the Earth to the unstable manifold of this periodic orbit. At the same time, when we consider the L_2 point of the Earth–Moon system, is has periodic orbits whose stable manifold "intersect" the unstable manifold that we have reached departing from the Earth and are temporarily cap-

tured by the Moon. With a second small Δv, we can force the intersection to behave as a true one.

The orbit computed in this way can be used as an intial guess to find a true solution, in the JPL ephemeris model, performing the prescribed acrobacies.

6.2. *Petit Grand Tour*

The general idea for the "Petit Grand Tour" of the Moons of Jupiter is similar to the one of "Shoot the Moon". In a first step, the Jovian moon n–body system is decoupled into several three–body systems. The tour starts close to the L_2 point of an outer moon (for instance Ganymede). Thanks to an heteroclinic connection between periodic orbits around L_1 and L_2, we can go from the vicinity of L_2 to the vicinity of L_1 and, in between, perform one o several loops around Ganymede. Now, we can look for "intersections" between the unstable manifold of the p.o. arond the L_1 point and the stable manifold of some p.o. around the L_2 point of some inner moon (for instance Europa). By the same considerations, we can turn around Europa and leave its influence through the L_1 point. Once the orbits have been obtained, they are easily refined to a more realistic model.

6.3. *Solar sytem low energy transfers and astronomical applications*

As Lo and Ross [52] suggested, the exploration of the phase space structure, as revealed by the homoclinic/heteroclinic structures and their association with mean motion resonances, may provide deeper conceptual insight into the evolution and structure of the asteroid belt (interior to Jupiter) anf the Kuiper belt (exterior to Neptune), plus the transport between these two belts and the terrestrial planet region.

Potential Earth–impacting asteroids may utilize the dynamical channels as a pathway to Earth from nearby heliocentric orbits in resonance with the Earth. This phenomenon has been observed recently in the impact of comet Shoemaker–Levy 9 with Jupiter, which was in 2:3 resonance with Jupiter just before impact.

Numerical simulations of the orbital evolution of asteroidal dust particles show that the earth is embedded in a circumsolar ring of asteroidal dust, known as the zodiacal dust cloud. Both simulations and observations reveal that the zodiacal dust cloud has structure. When viewed in the Sun–Earth rotating frame, there are several high density clumps which are mostly evenly distributed throughout Earth's orbit. The dust particles are belived to spiral towards the Sun from the asteroid belt, becoming trapped temporarily in exterior mean motion resonances with the Earth. It is suspected that the gross morphology of the ring is given by a simpler RTBP model involving the homoclinic and heteroclinic structures associated with the libration points.

7. Station keeping

7.1. *The Target mode approach and the Floquet mode approach*

The problem of controlling a spacecraft moving near an inherently unstable libration point orbit is of current interest. In the late 1960's, Farquhar [15] suggested several station–keeping strategies for nearly–periodic solutions near the collinear points. Later, in 1974, a station–keeping method for spacecraft moving on halo orbits in the vicinity of the Earth–Moon translunar libration point (L_2) was published by Breakwell, Kamel and Ratner [7]. These studies assumed that the control could be modeled as continuous. In contrast, specific mission requirements influenced the station–keeping strategy for the first libration point mission. Launched in 1978, the International Sun–Earth Explorer–3 (ISEE–3) spacecraft remained in a near–halo orbit associated with the interior libration point (L_1) of the Sun–Earth/Moon barycenter system for approximately three and one half years (Farquhar [18]). Impulsive maneuvers at discrete time intervals (up to 90 days) were successfully implemented as a means of trajectory control. Since that time, more detailed investigations have resulted in various station–keeping strategies, including the two identified here as the Target Point and Floquet Mode approaches.

The Target Point method (as presented by Howell and Pernicka [43], Howell and Gordon [39], and Keeter [47]) computes correction maneuvers by

minimizing a weighted cost function. The cost function is defined in terms of a corrective maneuver, as well as position and velocity deviations from a nominal orbit at a number of specified future times t_i. The non–final state vectors at each time t_i are denoted as "target points." The target points are selected along the trajectory at discrete time intervals that are downstream of the maneuver. In contrast, the Floquet Mode approach, as developed by Simó et al. [66,67], incorporates invariant manifold theory and Floquet modes to compute the maneuvers. Floquet modes associated with the monodromy matrix are used to determine the unstable component corresponding to the local error vector. The maneuver is then computed such that it eradicates the dominant unstable component of the error. It is noted that both approaches have been demonstrated in a complex model such as the Earth–Moon system.

Target Point Approach

The goal of the Target Point station–keeping algorithm is to compute and implement maneuvers to maintain a spacecraft "close" to the nominal orbit, i.e., within a region that is locally approximated in terms of some specified radius centered about the reference path. To accomplish this task, a control procedure is derived from minimization of a cost function. The cost function, J, is defined by weighting both the control energy required to implement a station–keeping maneuver, Δv, and a series of predicted deviations of the six–dimensional state from the nominal orbit at specified future times. The cost function includes several submatrices from the state transition matrix. For notational ease, the state transition matrix is partitioned into four 3×3 submatrices as

$$\Phi(t_k, t_0) = \begin{bmatrix} A_{k0} & B_{k0} \\ C_{k0} & D_{k0} \end{bmatrix}. \tag{19}$$

The controller, in this formulation, computes a Δv in order to change the deviation of the spacecraft from the nominal path at some set of future times. The cost function to be minimized is written in general as

$$J = \Delta v^T Q \Delta v + p_1^T R p_1 + v_1^T R_\nu v_1 + p_2^T S p_2 + v_2^T S_\nu v_2 + p_3^T T p_3 + v_3^T T_\nu v_3, \tag{20}$$

where superscript T denotes transpose. The variables in the cost function include the corrective maneuver, Δv, at some time t_c, and p_1, p_2 and p_3 that are defined as 3×1 column vectors representing linear approximations of the expected deviations of the actual spacecraft trajectory from the nominal

path (if no corrective action is taken) at specified future times t_1, t_2 and t_3, respectively. Likewise, the 3×1 vectors v_1, v_2 and v_3 represent deviations of the spacecraft velocity at the corresponding t_i. The future times at which predictions of the position and velocity state of the vehicle are compared to the nominal path are denoted as target points. They are represented as Δt_i such that $t_i = t_0 + \Delta t_i$. The choice of identifying *three* future target points is arbitrary.

In Eqn. (20), Q, R, S, T, R_ν, S_ν, and T_ν, are 3×3 weighting matrices. The weighting matrix Q is symmetric positive definite; the other weighting matrices are positive semi–definite. The weighting matrices are generally treated as constants that must be specified as inputs. Selection of appropriate weighting matrix elements is a trial and error process that has proven to be time–consuming. A methodology has been developed that automatically selects and updates the weighting matrices for each maneuver. This "time-varying" weighting matrix algorithm is based solely on empirical observations.

Determination of the Δv corresponding to the relative minimum of this cost function allows a linear equation for the optimal control input, i.e.,

$$
\begin{aligned}
&\Delta v^* = \\
&-\left[Q + B_{10}^T R B_{10} + B_{20}^T S B_{20} + B_{30}^T T B_{30} + D_{10}^T R_\nu D_{10} + D_{20}^T S_\nu D_{20} + D_{30}^T T_\nu D_{30}\right]^{-1} \\
&\times \left[\left(B_{10}^T R B_{10} + B_{20}^T S B_{20} + B_{30}^T T B_{30} + D_{10}^T R_\nu D_{10} + D_{20}^T S_\nu D_{20} + D_{30}^T T_\nu D_{30}\right) v_0\right. \\
&\left. + \left(B_{10}^T R A_{10} + B_{20}^T S A_{20} + B_{30}^T T A_{30} + D_{10}^T R_\nu C_{10} + D_{20}^T S_\nu C_{20} + D_{30}^T T_\nu C_{30}\right) p_0\right],
\end{aligned}
$$

where v_0, is the residual velocity (3×1 vector) and p_0 is the residual position (3×1 vector) relative to the nominal path at the time t_0. The performance of the modified Target Point algorithm is not yet truly "optimal," though it has been demonstrated to successfully control the spacecraft at reasonable costs. This accomplishment alone provides the user with a quick and efficient way to obtain reasonable station–keeping results. Given some procedure to select the weighting matrices, the maneuver is computed from the above equation. The corrective maneuver (Δv^*) is a function of spacecraft drift (in both position and velocity with respect to the nominal orbit), the state transition matrix elements associated with the nominal orbit, and the weighting matrices. It is assumed here that there is no delay in implementation of the maneuver; the corrective maneuver occurs at the time t_0, defined as the current time. Note that this general method could certainly

accommodate inclusion of additional target points. Although the nominal orbit that is under consideration here is quasiperiodic, the methodology does not rely on periodicity; it should be applicable to any type of motion in this regime.

In this application, three additional constraints are specified in the station–keeping procedure to restrict maneuver implementation. First, the time elapsed between successive maneuvers must be greater than or equal to a specified minimum time interval, t_{min}. This constraint may be regulated by the orbit determination process, scientific payload requirements, and/or mission operations. Time intervals of one to three days are considered in the Earth-Moon system. The second constraint is a scalar distance (p_{min}) and specifies a minimum deviation from the nominal path (an isochronous correspondence) that must be exceeded prior to maneuver execution. For distances less than p_{min}, maneuver computations do not occur. Third, in the station–keeping simulation, the magnitude of position deviations are compared between successive tracking intervals. If the magnitude is decreasing, a maneuver is not calculated. For a corrective maneuver to be computed, all three criteria must be satisfied simultaneously.

After a maneuver is calculated by the algorithm, an additional constraint is specified on the minimum allowable maneuver magnitude, Δv_{min}. lf the magnitude of the calculated — Δv is less than Δv_{min} then the recommended maneuver is cancelled. This constraint is useful in avoiding "small" maneuvers that are approximately the same order of magnitude as the maneuver errors. It also serves to model actual hardware limitations.

Floquet Mode Approach

An alternate strategy for station–keeping is the Floquet Mode approach, a method that is significantly different from the Target Point approach. It can be easily formulated in the circular restricted three–body problem. In this context, the nominal halo orbit is periodic. The variational equations for motion in the vicinity of the nominal trajectory are linear with periodic coefficients. Thus, in general, both qualitative and quantitative information can be obtained about the behavior of the nonlinear system from the monodromy matrix, M, which is defined as the state transition matrix (STM) after one revolution along the full halo orbit.

The knowledge of the dynamics of the flow around a halo orbit, or any solution close to it, allows other possibilities in addition to the station–keeping procedure described here, such as the computation of transfer orbits both between halo orbits and from the Earth to a halo orbit (Gómez *et al.* [21,29]). The behavior of the solutions in a neighborhood of the halo orbits is determined by the eigenvalues, λ_i, $i = 1, \ldots, 6$ and eigenvectors e_i, $i = 1, \ldots, 6$ of M. Gathering the eigenvalues by pairs, their geometrical meaning is the following:

a) The first pair (λ_1, λ_2) with $\lambda_1 \cdot \lambda_2 = 1$ and $\lambda_1 \approx 1500$, is associated with the unstable character of the small and medium size halo orbits. The eigenvector, $e_1(t_0)$, associated with the largest eigenvalue, λ_1, defines the most expanding direction, related to the unstable nature of the halo orbit. The image under the variational flow of the initial vector $e_1(t_0)$, together with the vector tangent to the orbit, defines the linear approximation of the unstable manifold of the orbit. In a similar way, $e_2(t_0)$ can be used to compute the linear approximation of the stable manifold.
b) The second pair $(\lambda_3, \lambda_4) = (1, 1)$ is associated with neutral variables (i.e., unstable modes). However, there is only one eigenvector with eigenvalue equal to one. This vector, $e_3(t_0)$ is the tangent vector to the orbit. The other eigenvalue, $\lambda_4 = 1$, is associated with variations of the energy (or the period) of the orbit through the family of halo orbits. Along the orbit, the vectors e_3 and e_4 span an invariant plane under the flow.
c) The third couple, (λ_5, λ_6), is formed by two complex conjugated eigenvectors of modulus one. The restriction of the flow to the corresponding two–dimensional invariant subspace, is essentially a rotation. This behavior is related to the existence of quasiperiodic halo orbits around the halo orbit (see Gómez *et al.* [33]).

When considering dynamical models of motion different from the restricted three–body problem, halo orbits are no longer periodic, and the monodromy matrix is not defined. Nevertheless, for quasiperiodic motions close to the halo orbit (and also for the Lissajous orbits around the equilibrium point) the unstable and stable manifolds subsist. The neutral behavior can be slightly modified including some instability which, from a practical point of view, is negligible when compared with the one associated with λ_1.

Instead of the vectors $e_i(t)$ it is convenient to use the Floquet modes $\overline{e}_i(t)$ which, for the periodic case, are defined as six periodic vectors from which the $e_i(t)$ can be easily recovered (see Wiesel [71]). For instance $\overline{e}_1(t)$ is defined as $e_1(t) \cdot \exp[-(t/T)\log\lambda_1]$, where T is the period of the halo orbit. The control algorithm is developed to utilize this information for station–keeping purposes. The emphasis is placed on formulating a controller that will effectively eliminate the unstable component of the error vector, $\delta(t) = (\delta x, \delta y, \delta z, \delta\dot{x}, \delta\dot{y}, \delta\dot{z})$ defined as the difference between the actual coordinates obtained by tracking and the nominal ones computed isochronously on the reference orbit. At any epoch, t, δ can be expressed in terms of the Floquet modes

$$\delta(t) = \sum_{i=1}^{6} \alpha_i \overline{e}_i(t). \tag{21}$$

The controller objective is to add a maneuver such that the magnitude of the component of the error vector in the unstable direction, α_1, is reduced to zero. The five remaining components do not produce large departures from the reference orbit. By contrast, the component of the error vector along the unstable mode increases by a factor of λ_1 in each revolution.

Denoting the impulsive maneuver as $\Delta = (0, 0, 0, \Delta_x, \Delta_y, \Delta_z)^T$, to cancel the unitary unstable Floquet mode, it is required that

$$\frac{\overline{e}_1}{\|\overline{e}_1\|} + (0, 0, 0, \Delta_x, \Delta_y, \Delta_z)^T = \sum_{i=2}^{6} c_i \overline{e}_i(t). \tag{22}$$

From these equations Δ_x, Δ_y, Δ_z can be obtained as a function of c_5 and c_6. These free parameters are determined by either imposing a constraint on the available directions of the control or by minimizing a suitable norm of Δ.

For practical implementation it is useful to compute the so–called projection factor along the unstable direction. It is defined as the vector π such that $\delta \cdot \pi = \alpha_1$. Note that for the computation of π only the Floquet modes are required, so it can be computed and stored together with the nominal orbit. To annihilate the unstable projection, α_1, with a maneuver, $\Delta v = (0, 0, 0, \Delta_x, \Delta_y, \Delta_z)^T$, we ask $(\delta + \Delta v) \cdot \pi = 0$. In this way,

$$\Delta_x \pi_4 + \Delta_y \pi_5 + \Delta_z \pi_6 + \alpha_1 = 0 \tag{23}$$

is obtained, where π_4, π_5 and π_6 are the last three components of π. Choosing a two axis controller, with $\Delta_z = 0$, and minimizing the Euclidean norm of Δv, the following expressions for Δ_x and Δ_y are obtained,

$$\Delta_x = -\frac{\alpha_1 \pi_4}{\pi_4^2 + \pi_5^2}, \quad \Delta_y = -\frac{\alpha_1 \pi_5}{\pi_4^2 + \pi_5^2}. \tag{24}$$

In a similar way, a one or three axis controller can be formulated.

Once the magnitude of the maneuver is known, an important consideration is the determination of the epoch at which it must be applied. The study of this question requires the introduction of the gain function, $g(t) = \|\Delta\|^{-1}$, where Δ is the unitary impulsive maneuver. It measures the efficiency of the control maneuver along the orbit to cancel the unitary unstable component. This component is obtained using the projection factors and the error vector. As the projection factor changes along the orbit, the same error vector has different unstable components. It is natural then to consider a delay in the maneuver until reaching a better epoch with less cost. So, the function to be studied is

$$R(t) = \frac{\exp\left(t \log\left(\frac{\lambda_1}{T}\right)\right)}{g(t)}. \tag{25}$$

However, as is shown in Simó *et al.* [66], this function is always increasing, therefore, it is never good to wait for a maneuver except for operational reasons.

As it has been said, when the station keeping has to span for a long time, the satellite can tend to deviate far away from the nominal orbit. This could happen since the cancellation of the unstable component does not take care of the neutral components which might grow up to the limit of loosing controllability. In order to prevent large deviations of the satellite from the nominal orbit, it is advisable to perform manoeuvres of insertion in the stable manifold. The main idea of the strategy is to put the satellite in a state such that approaches the nominal orbit assimptotically in the future. This strategy is in principle much cheaper than to target to the nominal orbit itself since the latter case can be considered, from an implementation point of view, as a sub-case of targeting to the stable manifold. Moreover, even when the controllability using only unstable component cancellation manoeuvres (UCCM) is assured, it can be advantageous to perform insertion in the stable manifold since the control effect of this manoeuvres usually persist for a longer time span than UCCM. Moreover, subsequent

UCCM would be cheaper due to the fact that the satellite is closer to the nominal orbit, and consequently the projection of the deviation in the unstable component is smaller.

Although the idea is simple, the implementation is not so easy since in first place, the target state in the stable manifold cannot be accomplished with a single manoeuvre as it happens with UCCM and, in second place, the actual state of the satellite is known but affected by tracking errors. Moreover the manoeuvres to be done will be noised by some errors too. We refer the interested reader to Gómez *et al.* [31] for the details of the implementation.

As a final remark, several constraints that impact the maneuvers must be specified in the procedure. The most relevant are the time interval between two consecutive tracking epochs (tracking interval), the minimum time interval between maneuvers, and the minimum value of α_1 that cannot be considered due solely to tracking errors.

Special emphasis must be placed on the evolution of α_1. With no tracking errors, the evolution of this parameter is exponential with time (see Figures 13 and 14). When adding tracking errors, and in order to prevent a useless maneuver, this value must be greater than the minimum. So, the minimum value must be selected as a function of the accuracy in orbit determination. On the other hand, the value of α_1 should not be too large, because this increases the value of the maneuver in an exponential way. Thus, a maximum value is chosen such that, if α_1 is greater than the maximum, a control maneuver will be executed to cancel the unstable component. When α_1 is between the minimum and maximum values, the error can be due to small oscillations around the nominal orbit. In this case, a maneuver is executed only if the error has been growing at an exponential rate in the previous time steps and the time span since the last maneuver agrees with the one selected. Also, if the magnitude of the calculated Δv is less than Δv_{min}, then the recommended maneuver is cancelled. Once these parameters have been fixed, there are no more free variables allowing any further minimization.

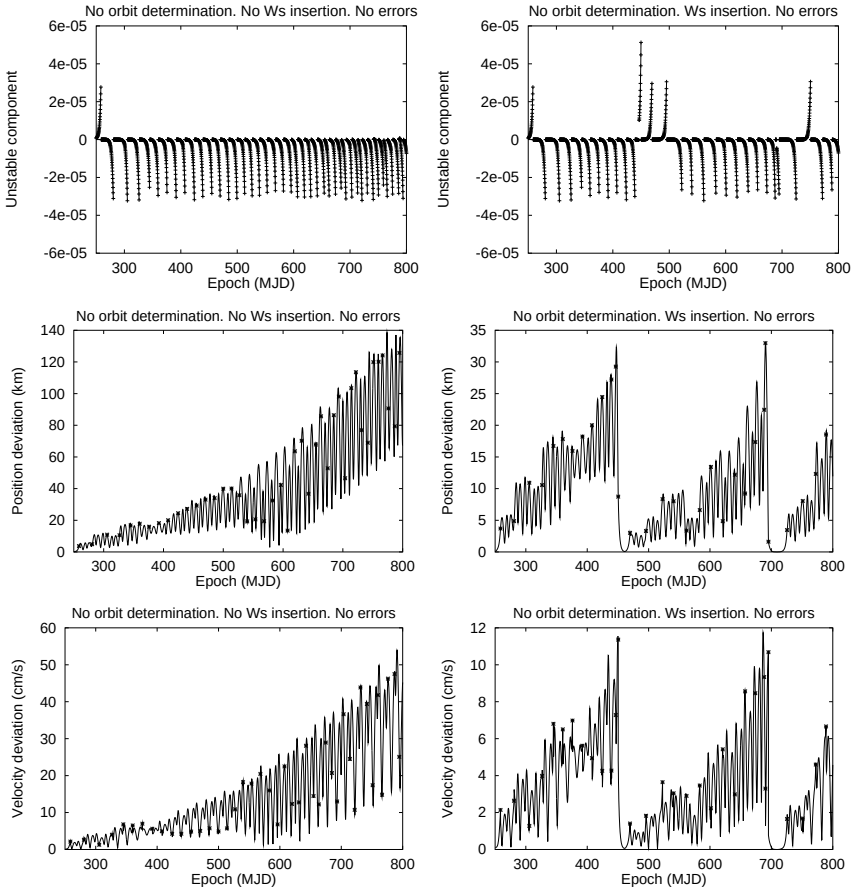

Fig. 13. From top to bottom, evolution with time of the unstable component, position deviations with respect to the nominal trajectory, and velocity deviations. In all the figures, no orbit determination has been performed, because the simulations have been done with no errors for the tracking and the execution of the manoeuvres. There is only an error at the initial insertion epoch. In the left hand side figures there are no manoeuvres for the insertion in the stable manifold, while in the right hand side there are. These manoeuvres can be clearly seen, because after its execution the distance to the nominal orbit goes to zero both in position and in velocity. The discontinuities that appear in these two figures are associated to the execution of the manoeuvres. The points marked with a cross are those at which the tracking has been performed, and the ones marked with a star are those at which a manoeuvre has been executed.

7.2. *Numerical results*

In Figures 13 and 14, we show some results of simulations done for a halo orbit around L_2 in the Earth-Moon system. We display the evolution of

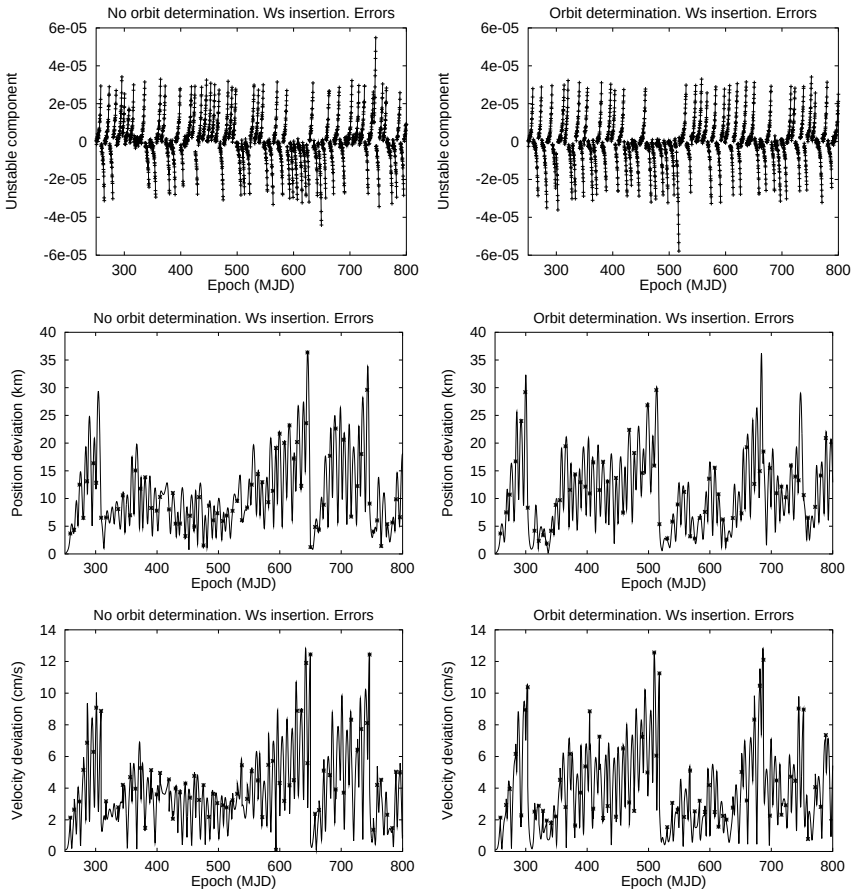

Fig. 14. From top to bottom, evolution with time of the unstable component, position deviations with respect to the nominal trajectory, and velocity deviations. In the left figures no orbit determination if performed, while in the right ones it is done. In all the figures, the manoeuvres and the tracking are performed with errors. There is also an error at the initial insertion epoch. There are manoeuvres for the insertion in the stable manifold that can be clearly seen at the times at which the distance to the nominal orbit decreases to very small values (which are not equal to zero because there is an error added to the manoeuvres). The points marked with a cross are those at which the tracking has been performed, and the ones marked with a star are those at which a manoeuvre has been executed.

the unstable component and the deviations from the nominal trajectory in position and velocity in different situations. In Figure 13 the manoeuvres are done without any error, while in Figure 14 they are performed with errors.

In each Figure, we show the results of the station keeping strategy with and without stable manifold insertion manoeuvres. From them, it becomes clear both the exponential grow of α_1 and the role of the insertion manifold manoeuvres.

Finally, in Figure 15 the averaged Δv used for the station keeping is displayed. As before, the simulations correspond to a halo orbit around L_2 in the Earth-Moon system. If no insertion manifold manoeuvres are done, there appears an exponential grow of the Δv, while if these manoeuvres are done, the station keeping cost per year remains constant. From this Figure, it is also clear that a good orbit determination procedure can be useful to reduce the total Δv.

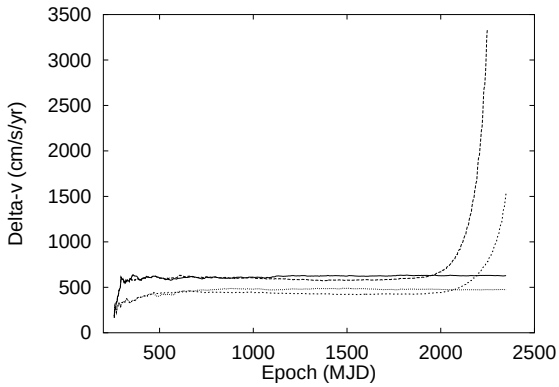

Fig. 15. Averaged Δv used for the station keeping, in cm/s/year, in different situations. The two curves with an exponential grow of the Δv correspond to simulations with no insertions in the stable manifold. For the upper curve, there was no orbit determination. For the other two curves, for which there seems to be a finite limit for the Δv, we have used insertion maneuvers in the stable manifold. The one with lower cost uses orbit determination, whereas the other does not.

8. Application of libration point orbits to formation flight

The excellent observational properties of the L_2 point of the Earth–Sun system have lead to consider this location for missions requiring a flying multiple spacecraft in a controlled formation. Darwing, LISA and TPF are three of the more challenging examples of such missions.

Two basic orbital strategies have been analyzed for a formation flying mission at the libration points: a *nominal orbit strategy* and a *base orbit strategy*. In the nominal orbit strategy each spacecraft follows its own predefined orbit, while in the base orbit strategy each spacecraft follows an orbit relative to a predefined one, known as the base orbit. The base orbit may have no spacecraft on it. In the next two sections we will briefly discuss the results that have been obtained in both approaches.

8.1. *The nominal orbit strategy*

Barden and Howell [3,4,38] have considered the possibility of using quasi–periodic solutions around the halo orbits and the libration points, as natural locations for a constellation. In their studies, a certain number of spacecraft are initially placed along a planar curve close to any of the two kinds of the above mentioned tori and, in a first step, they analyze their natural motion.

In the quasi-halo case, the torus itself is related to an underlying periodic halo orbit. As the initial planar curve proceeds in time along the torus, in the direction of motion of the underlying halo orbit, there are certain aspects of the evolution of the curve that are of particular interest. The curve appears simply closed and nearly circular in configuration space. When the amplitude of the curve is small, i.e., less than 1000 km, the curve is considered to be planar. However, as the curve evolves, it changes size and shape. Identifying the plane containing the curve, one can view the constellation from a point along the normal to the plane. Although the plane will not persist, the deviations from a reference one are small: less than 1% of the distance between spacecraft when they are on opposite sides of the constellation. In addition to the variations in size and shape, there is a winding aspect of the motion due to the change of the relative locations of the points of the curve. This is because the torus is self–intersectiong in the configuration space at the two xz-plane crossings.

This type of natural motion, as an option for formation flying, is very appealing from a dynamical perspective. From a practical standpoint, however, this formation will likely not meet the constraints and scientific requirements of a generic mission. The likely scenario is that some prespecified formation will be mandated.

As an example of non-natural formation, Barden and Howell consider six spacecraft evenly distributed on a circle of radius 100 km in a plane coincident with the rotating libration point coordinates y and z (parallel to the yz plane) and around a Lissajous type orbit. At each maneuver, the formation is enforced to be on the plane, but there will be out-off-plane excursions for each of the spacecrafts between the maneuvers; the amplitude of the excursions will vary for each vehicle. In a first simulation, four maneuvers per revolution in the xy plane (nearly equally spaced in time) are executed where all six spacecraft implement their respective maneuvers simultaneously. The size of the maneuvers ranges from 0.043 m/s to 0.12 m/s for a total cost of 2.93 m/s for a duration of 355 days (which is equivalent to two revolutions along the baseline Lissajous trajectoy in the xy plane. These maneuvers are necessary to define a nominal path for each of the spacecraft; additional stationkeeping maneuvers will also be required to accommodate errors and uncertainties. Even for the baseline motion, however, out-of-plane excursions between the maneuvers reach a maximum value at any one time of approximately 20 km in this example. The only means of reducing this deviation is to increase the frequency of the maneuvers. With maneuvers every 11 days, instead of 44 days, the out-of-plane deviations never exceed 1.8 km. The total cost is of 2.77 m/s which is smaller than the 2.93 m/s required. However, fixed planes can be specified where the total cost increases with the increased number of maneuvers.

8.2. *Formation flight in the vicinity of a libration point. TPF case*

The TPF Mission (Terrestrial Planet Finder) is one of the center pieces of the NASA Origins Program. The goal of TPF is to identify terrestrial planets around stars nearby the Solar System (see Beichman *et al.* [5]). For this purpose, a space-based infrared interferometer with a baseline of approximately 100 m is required. To achieve such a large baseline, a distributed system of five spacecraft flying in formation is an efficient approach. Since the TPF instruments needs a cold and stable environment, near Earth orbits are unsuitable. Two potential orbits have been identified: a SIRTF-like heliocentric orbit and a libration orbit near the L_2 Lagrange point of the Earth-Sun system. There are several advantages to a libration orbit near L_2. Such orbits are easy and inexpensive to get to from Earth. Moreover, for missions with heat sensitive instruments (e.g. IR detectors), libration orbits

provide a constant geometry for observation with half of the entire celestial sphere available at all times. The spacecraft geometry is nearly constant, with Sun, Earth, and Moon always behind the spacecraft, thereby providing a stable observation environment, making observation planning much simpler. In this section we present some of the results of Gómez *et al.* [20], which contain preliminary computations of the TPF mission.

From the dynamical point of view, the TPF Mission can be broken into four scenarios:

Launch and Transfer Phase

For the simulation, it is assumed that the spacecraft starts in a typical 200 km altitude parking orbit at 28.5 deg inclination, and a halo orbit is used as a target Baseline Orbit. At the appropriate time, the spacecraft performs a major maneuver of about 3200 m/s. This injects the spacecraft onto the stable manifold of the halo orbit to begin the Transfer Phase. The transfer trajectory is designed by using an orbit of the stable manifold with a suitable close approach to the Earth.

Deployment Phase

It is assumed that all the spacecraft of the formation reach the Baseline Orbit in a single spacecraft. This begins the Deployment Phase. The five satellites are maneuvered to reach their initial positions on the different points of a 20-gon of 100m diameter at the same time. The Deployment Phase can last several hours and simulations between 1 and 10 hours have been done. Assuming that deployment is performed using two impulsive maneouvres, and that a selected satellite has to be put in the edge of an 20-gon of diameter D meters, and after that starts doing R revolutions per day, the following table summarizes the estimation of the deployment cost in cm/s as a function of the deployment time.

Deployment Time	$R = 1$	$R = 3$
1 Hr	$5.5 \times 10^{-2}\, D$	$5.6 \times 10^{-2}\, D$
3 Hr	$1.9 \times 10^{-2}\, D$	$2.7 \times 10^{-2}\, D$
5 Hr	$1.3 \times 10^{-2}\, D$	$2.2 \times 10^{-2}\, D$
10 Hr	$0.9 \times 10^{-2}\, D$	$1.8 \times 10^{-2}\, D$
100 Hr	$0.5 \times 10^{-2}\, D$	$1.5 \times 10^{-2}\, D$

Pattern Maintenance Phase

Once the initial configuration has been established, the spacecraft will manoeuvre to follow the edge of the 20-gon to provide a suitable spin rate for the formation. The nominal spin rate used for this simulation is 360 deg every 8 hours. The period where the pattern is maintained is called the Pattern Maintenance Phase. Assuming that a spacecraft is spining in a 20-gon of diameter D meters and doing R revoulitions per day, it is obtained that:

$$\text{Formation maintenance cost per satellite in cm/s per Day} = 0.0023\, D\, R^2.$$

Reconfiguration Phase

Once sufficient data has been acquired for one star system, the formation will be pointed to another star for observation. Repointings occur during the Reconfiguration Phase. The computations of the Reconfiguration Phase cost is similar to the Deployment Phase, except that the spacecraft do not depart from the same location (i.e. the Mother Ship).

Estimation of TPF budget for a ten year's mission

A table presenting an estimation of the ΔV cost associated to satellites located in an N-gon of 50 and 100 m around a L_2 base halo orbit, spining at the rate of 3 revolutions per day, for a 10 years mission is also given.

Maneuvers per S/C in m/s	50m Diameter Case	100m Diameter Case
Halo Insertion	5	5
Initial Deployment (10h)	0.009	0.018
Formation Maintenance	0.1/Day	0.2/Day
Station Keeping (Z-Axis)	3/Yr	3/Yr
Reconfiguration (est.)	0.05/Day	0.1/Day
10 Year DV Budget (m/s)	585	1135

Halo insertion cost, due to transfer from the Earth, and station keeping cost (including avoidance of the exclusion zone, that could be required in case of using an L_2 Lissajous orbit) are also included. The usual station keeping can be assumed to be absorbed in the so often performed pattern maintenance manoeuvres. Manoeuvres are also considered to be done

without error, so control correction maneuvers are not included. Finally, the paper ends with some issues related to the TPF simulations and the visualization tools suitable for the design of the mission.

Acknowledgments

The work has been partially supported by DGICYT grant PB94–0215 and CIRIT grant 2000 SGR–27. The authors are indebted to their colleages K. Howell, À. Jorba, W.S. Koon, J. Llibre, M.W. Lo, J.E. Marsden, R. Martínez, S. Ross, and, very specially, to C. Simó, with whom they have done most of the work contained in this review paper.

References

1. M.A. Andreu: *The Quasibicircular Problem*. PhD thesis, Dept. Matemàtica Aplicada i Anàlisi, Universitat de Barcelona, Barcelona, Spain, 1999.
2. M.A. Andreu: Dynamics in the Center Manifold Around l_2 in the Quasi-Bicircular Problem. *Celestial Mechanics and Dynamical Astronomy*, 84(2):105–133, 2002.
3. B.T. Barden and K.C. Howell: Formation Flying in the Vicinity of Libration Point Orbits. In *AAS Paper 98-169, Monterey, CA.*, 1998.
4. B.T. Barden and K.C. Howell: Dynamical Issues Associated with Relative Configurations of Multiple Spacecraft near the Sun–Earth/Moon l_1 Point. In *AAS Paper 99-450, Girdwood, Alaska.*, 1999.
5. C.A. Beichman, N.J. Wolf and C.A. Lindensmith: *The Terrestrial Planet Finder (TPF)*. JPL Publications 99–003, 1999. (http://tpf.jpl.nasa.gov).
6. E. Belbruno and J. Miller: Sun-Perturbed Earth to Moon Transfers with Ballistic Capture. *Journal of Guidance, Control and Dynamics*, 16:770–775, 1993.
7. J.V. Breakwell, A.A. Kamel and M.J. Ratner: Station-Keeping for a Translunar Communications Station. *Celestial Mechanics*, 10(3):357–373, 1974.
8. E. Castellà and À. Jorba: On the Vertical Families of Two-Dimensional Tori Near the Triangular Points of the Bicircular Problem. *Celestial Mechanics and Dynamical Astronomy*, 76:35–54, 2000.
9. J. Cobos and M. Hechler: FIRST Mission Analysis: Transfer to Small Lissajous Orbits around L_2. Technical Report MAS Working Paper No. 398, ESOC, 1997.
10. J. Cobos and J.J. Masdemont: Astrodynamical Applications of Invariant Manifolds Associated with Collinear Lissajous Libration Orbits. In *Libration Point Orbits and Applications*, 2003.

11. J. Cobos and J.J. Masdemont: Transfers Between Lissajous Libration Point Orbits. Technical report, In preparation.
12. A. Deprit: Canonical Transformations Depending on a Small Parameter. *Celestial Mechanics*, 1(1):12–30, 1969.
13. E.J. Doedel, R.P. Paffenroth, H.B. Keller, D.J. Dichmann, J. Galán-Vioque, and A. Vanderbauwhede: Computation of Periodic Orbits of Conservative Systems with Applications to the 3–body Problem. *Int. J. Bifurcation and Chaos*, 2002.
14. N. Eismont, D. Dunham, J. Sho-Chiang and R.W. Farquhar: Lunar Swingby as a Tool for Halo–Orbit Optimization in Relict–2 Project. In *Third International Symposium on Spacecraft Flight Dynamics, ESA SP–326*. European Space Agency (Darmstadt, Germany), 1991.
15. R.W. Farquhar: Far Libration Point of Mercury. *Astronautics & Aeronautics*, 5(8):4, 1967.
16. R.W. Farquhar: The Control and Use of Libration Point Satellites. Technical Report TR R346, Stanford University Report SUDAAR–350 (1968). Reprinted as NASA, 1970.
17. R.W. Farquhar: The Moon's Influence in the Location of the Sun–Earth Exterior Libration Point. *Celestial Mechanics*, 2(2):131–133, 1970.
18. R.W. Farquhar, D.P. Muhonen, C.R. Newman and H.S. Heuberger: Trajectories and Orbital Maneuvers for the First Libration–Point Satellite. *Journal of Guidance and Control*, 3(6):549–554, 1980.
19. F. Gabern and À. Jorba: A Restricted Four-Body Model for the Dynamics near the Lagrangian Points of the Sun-Jupier System. *Discrete and Continuous Dynamical Systems. Series B*, 1(2):143–182, 2001.
20. G. Gómez, M.W. Lo, J.J. Masdemont and K. Museth: Simulation of formation flight near l_2 for the tpf mission. In *ASS/AIAA Space Flight Mechanics Conference. Paper AAS 01-305*, 2001.
21. G. Gómez, À. Jorba, J. Masdemont and C. Simó: Study of the Transfer from the Earth to a Halo Orbit Around the Equilibrium Point L_1. *Celestial Mechanics*, 56(4):541–562, 1993.
22. G. Gómez, À. Jorba, J.J. Masdemont and C. Simó: Moon's Influence on the Transfer from the Earth to a Halo Orbit. In A. E. Roy, editor, *Predictability, Stability and Chaos in N-Body Dynamical Systems*, pages 283–290. Plenum Press, 1991.
23. G. Gómez, À. Jorba, J.J. Masdemont and C. Simó: *Dynamics and Mission Design Near Libration Point Orbits – Volume 3: Advanced Methods for Collinear Points*. World Scientific, 2001.
24. G. Gómez, À. Jorba, J.J. Masdemont and C. Simó: *Dynamics and Mission Design Near Libration Point Orbits – Volume 4: Advanced Methods for Triangular Points*. World Scientific, 2001.
25. G. Gómez, W.S. Koon, M.W. Lo, J.E. Marsden, J.J. Masdemont and S.D. Ross: Invariant Manifolds, the Spatial Three-Body Problem and Space Mission Design. *Advances in The Astronautical Sciences*, 109, 1:3–22, 2001.
26. G. Gómez, J. Llibre, R. Martínez and C. Simó: *Dynamics and Mission Design Near Libration Point Orbits – Volume 1: Fundamentals: The Case of*

Collinear Libration Points. World Scientific, 2001.
27. G. Gómez, J. Llibre and J. Masdemont: Homoclinic and Heteroclinic Solutions in the Restricted Three-Body Problem. *Celestial Mechanics*, 44:239–259, 1988.
28. G. Gómez, M. Marcote and J.J. Masdemont: Trajectory Correction Manoeuvres in the Transfer to Libration Point Orbits. In these Proceedings.
29. G. Gómez, J. Masdemont and C. Simó: Study of the Transfer Between Halo Orbits. *Acta Astronautica*, 43(9–10):493–520, 1998.
30. G. Gómez and J.J. Masdemont: Some Zero Cost Transfers Between Halo Orbits. *Advances in the Astronautical Sciences*, 105(2):1199–1216, 2000.
31. G. Gómez and J.J. Masdemont: Refinements of a Station–Keeping Strategy for Libration Point Orbits. In preparation, 2002.
32. G. Gómez, J.J. Masdemont and J.M. Mondelo: Solar System Models with a Selected Set of Frequencies. *Astronomy & Astrophysics*, 390:733–749, 2002.
33. G. Gómez, J.J. Masdemont and C. Simó: Quasihalo Orbits Associated with Libration Points. *Journal of The Astronautical Sciences*, 46(2):1–42, 1999.
34. G. Gómez and J.M. Mondelo: The Dynamics Around the Collinear Equilibrium Points of the RTBP. *Physica D*, 157(4):283–321, 2001.
35. M. Hechler: SOHO Mission Analysis L_1 Transfer Trajectory. Technical Report MAO Working Paper No. 202, ESA, 1984.
36. L.A. Hiday and K.C. Howell: Transfers Between Libration–Point Orbits in the Elliptic Restricted Problem. In *AAS/AIAA Spaceflight Mechanics Conference, Paper AAS 92-126.*, 1992.
37. K.C. Howell and B.T. Barden: Brief Summary of Alternative Targeting Strategies for TCM1, TCM2 and TCM3. Private communication. Purdue University, 1999.
38. K.C. Howell and B.T. Barden: Trajectory Design and Station Keeping for Multiple Spacecraft in Formation Near de Sun-Earth L_1 Point. In *General Conference of the International Astronautical Federation. Paper IAF-99-A.7.07*, 1999.
39. K.C. Howell and S.C. Gordon: Orbit Determination Error Analysis and a Station–Keeping Strategy for Sun–Earth L_1 Libration Point Orbits. *Journal of the Astronautical Sciences*, 42(2):207–228, April–June 1994.
40. K.C. Howell and J.J. Guzman: Spacecraft Trajectory Design in the Context of a Coherent Restricted Four–Body problem with Application to the MAP Mission. In *Congress of the International Astronautical Federation*, volume IAF Paper 00–A.5.06, 2000.
41. K.C. Howell and L.A. Hiday-Johnston: Time-Free Transfers Between Libration-Point Orbits in the Elliptic Restricted Problem. *Acta Astronautica*, 32:245–254, 1994.
42. K.C. Howell, B.G. Marchand and M.W. Lo: Temporary Satellite Capture of Short–Period Jupiter Family Comets from the Perspective of Dynamical Systems. In *AAS/AIAA Space Flight Mechanics Meeting, AAS Paper 00-155*, 2000.
43. K.C. Howell and H.J. Pernicka: Stationkeeping Method for Libration Point Trajectories. *Journal of Guidance, Control and Dynamics*, 16(1):151–159,

1993.
44. À. Jorba: *Quasiperiodic Perturbations of Ordinary Differential Equations*. PhD thesis, Universitat de Barcelona, Barcelona, Spain, 1991.
45. À. Jorba and J.J. Masdemont: Dynamics in the Center Manifold of the Restricted Three–Body Problem. *Physica D*, 132:189–213, 1999.
46. À. Jorba and J. Villanueva: On the Normal Behaviour of Partially Elliptic Lower Dimensional Tori of Hamiltonian Systems. *Nonlinearity*, 10:783–822, 1997.
47. T.M. Keeter: Station–Keeping Strategies for Libration Point Orbits: Target Point and Floquet Mode Approaches. Master's thesis, School of Aeronautics and Astronautics, Purdue University, West Lafayette, Indiana, 1994.
48. W.S. Koon, M.W. Lo, J.E. Marsden and S.D. Ross: Heteroclinic Connections Between Periodic Prbits and Resonance Transitions in Celestial Mechanics. *Chaos*, 10(2):427–469, 2000.
49. W.S. Koon, M.W. Lo, J.E. Marsden and S.D. Ross: Low Energy Transfer to the Moon. *Celestial Mechanics and Dynamical Astronomy*, 81(1):63–73, 2001.
50. W.S. Koon, M.W. Lo, J.E. Marsden and S.D. Ross: Resonance and capture of jupiter comets. *Celestial Mechanics and Dynamical Astronomy*, 81(1):27–38, 2001.
51. D.F. Lawden: *Optimal Trajectories for Space Navigation*. Butterworths & Co. Publishers, London, 1963.
52. M.W. Lo and S. Ross: SURFing the Solar Sytem: Invariant Manifolds and the Dynamics of the Solar System. Technical Report 312/97, 2-4, JPL IOM, 1997.
53. M.W. Lo, B.G. Williams, W.E. Bollman, D. Han, Y. Hahn, J.L. Bell, E.A. Hirst, R.A. Corwin, P.E. Hong, K.C. Howell, B.T. Barden and R.S. Wilson: Genesis Mission Design. In *AIAA Space Flight Mechanics, Paper No. AIAA 98–4468*, 1998.
54. J.J. Masdemont: *Estudi i Utilització de Varietats Invariants en Problemes de Mecànica Celeste*. PhD thesis, Universitat Politècnica de Catalunya, Barcelona, Spain, 1991.
55. J.M. Mondelo: *Contribution to the Study of Fourier Methods for Quasi–Periodic Functions and the Vicinity of the Collinear Libration Points*. PhD thesis, Dept. Matemàtica Aplicada i Anàlisi, Universitat de Barcelona, Barcelona, Spain, 2001.
56. J.R. Pacha: *On the Quasi–Periodc Hamiltonian Andronov–Hopf Bifurcation*. PhD thesis, Dept. de Matemàtica Aplicada I, Universitat Politècnica de Catalunya, Barcelona, Spain, 2002.
57. D.L. Richardson: Analytical Construction of Periodic Orbits About the Collinear Points. *Celestial Mechanics*, 22(3):241–253, 1980.
58. D.L. Richardson: A note on the Lagrangian Formulation for Motion About the Collinear Points. *Celestial Mechanics*, 22(3):231–235, 1980.
59. R.S. Wilson, K.C. Howell and M.W. Lo: Optimization of Insertion Cost Transfer Trajectories to Libration Point Orbits. *Advances in the Astronautical Sciences*, 103:1569–1586, 2000.

60. D.J. Scheeres: The Restricted Hill Four–Body Problem with Applications to the Earth–Moon–Sun System. *Celestial Mechanics and Dynamical Astronomy*, 70(2):75–98, 1998.
61. R. Serban, W.S. Koon, M.W. Lo, J.E. Marsden, L.R. Petzold, S.D. Ross and R.S. Wilson: Halo Orbit Mission Correction Maneuvers Using Optimal Control. *Automatica*, 38:571–583, 2002.
62. C.L. Siegel and J.K. Moser: *Lectures on Celestial Mechanics*. Springer–Verlag, 1971.
63. C. Simó: Effective Computations in Hamiltonian Dynamics. In Société Mathématique de France, editor, *Cent ans après les Méthodes Nouvelles de H. Poincaré*, pages 1–23, 1996.
64. C. Simó: Dynamical Systems Methods for Space Missions on a Vicinity of Collinear Libration Points. In C. Simó, editor, *Hamiltonian Systems with Three or More Degrees of Freedom*, pages 223–241. Kluwer Academic Publishers, 1999.
65. C. Simó, G. Gómez, À. Jorba and J. Masdemont: The Bicircular Model Near the Triangular Libration Points of the RTBP. In A. Roy and B. Steves, editors, *From Newton to Chaos*, pages 343–370. Plenum Press, 1995.
66. C. Simó, G. Gómez, J. Llibre and R. Martínez: Station Keeping of a Quasiperiodic Halo Orbit Using Invariant Manifolds. In *Second International Symposium on Spacecraft Flight Dynamics*, pages 65–70. European Space Agency, Darmstadt, Germany, October 1986.
67. C. Simó, G. Gómez, J. Llibre, R. Martínez and R. Rodríquez: On the Optimal Station Keeping Control of Halo Orbits. *Acta Astronautica*, 15(6):391–397, 1987.
68. C. Simó and T.J. Stuchi: Central Stable/Unstable Manifolds and the Destruction of KAM Tori in the Planar Hill Problem. *Physica D*, 140(1–2):1–32, 2000.
69. J. Stoer and R. Bulirsch: *Introduction to Numerical Analysis*. Springer Verlag, 1983.
70. V. Szebehely: *Theory of Orbits*. Academic Press, 1967.
71. W. Wiesel and W. Shelton: Modal Control of an Unstable Periodic Orbit. *Journal of the Astronautical Sciences*, 31(1):63–76, 1983.